Supporting Information for

BesC Initiates C–C Cleavage through a Substrate-Triggered and Reactive Diferric-Peroxo Intermediate.

Olivia M. Manley,[a] Haoyu Tang,[b] Shan Xue,[c] Yisong Guo,[c] Wei-chen Chang,[b] and Thomas M. Makris[a,b,*]

[a]Departments of Molecular and Structural Biochemistry and [b]Chemistry, North Carolina State University, Raleigh, NC 27695. [c]Department of Chemistry, Carnegie Mellon University, Pittsburgh PA 15213

This PDF file includes:

Table of Contents

Materials and Methods

Reagents. Growth medium components, IPTG, and glycerol were purchased from Research Products International. Imidazole, HEPES, and kanamycin were purchased from Bio Basic, Inc. Iron (III) chloride, methyl viologen dichloride, α-ketoglutaric acid (αKG), L-lysine, and $^{18}O_2$ gas were purchased from Sigma-Aldrich. Oxygen and nitrogen gases were supplied by Arc3 Gases. Sodium chloride, organic solvents, and other common reagents were obtained from VWR/Avantor. ^{57}Fe and ^{18}O-water were obtained from Cambridge Isotope Laboratories, Inc. 4,4,5,5-d_4-L-lysine and 3,3,4,4,5,5,6,6-d_8 L-lysine were purchased from CDN Isotopes.

Expression and purification of BesC. The *besC* gene from *Streptomyces cattleya* was codon-optimized, synthesized, and subcloned into pET28b(+) with NdeI and HindIII restriction enzymes by Bio Basic for expression with an *N*-terminal hexahistidine tag. The final coding sequence follows:

```
ATGACCGACCTGAACACCCCGGAATCTACCTCTAAACCGGTTTGGGAACACTTCGACCACGTTGAACCGGGTATCCG
TCGTCGTATCGCGGTTGCGGACCCGGAAATCAAAGAATACCTGGACGGTATGCTGGCTCGTATCGCTTCTCACCGTG
GTGTTGAACACCCGTTCCTGAACGCGTACCGTACCACCGCACTGGACCCGGAACAGGAACGTCACCTGTTCTCTGAA
TGTTACTACTTCTTCCGTTATCTGCCGTTCTACATTACTGGTATGGCTGTTAAAACCCGTGATGAAATGATCCTGCG
TGAAATCATCCTGAACGTTGCGGATGAAGTTGGCTCTGATCCGACTCATTCTACCCTGTTCGCTGATTTCCTGGCTC
GTATTGGTATTGATAAAGAACACCTGGACGGTTACCAGCCGCTGGAAGTAACTCGTCAGCTGAACGACGGTATCCGT
CACCTGTACACCGAAACCTCTATCAACAAAGCTCTGGGTGCACTGTACGCTGATGAAACCATGAGCAGCATCATGGT
TAGCAAAATTAACGACGGTCTGCGTAACCAGGGTTATGATGACGACCTGCGTCACTTCTGGCAGCTGCACATCGATG
TTGAAGTTGGTCACTCTAACTCTGTTTTCAACGCTATCGCGCCGTACGTTGGCTCTAAAGCTGCGCGTGCTGAATTT
GAAGAAGGTGTTTTCGAATTTCTGGGTCTGGTTGAACGTTACTGGGATGGTGTTCGTGAACTGGTTGGTATCGGTAA
ATAA
```

The plasmid was transformed into *Escherichia coli* BL21(DE3) cells and plated on LB-agar plates containing 50 μg/mL kanamycin, from which a starter culture in LB media was made. The starter culture was used to inoculate 1-L cultures of LB media with 50 μg/mL kanamycin. The cultures were incubated at 37 °C while shaking at a speed of 200 rpm until they reached an $OD_{600\ nm}$ of 0.6-0.8, at which point the cultures were cooled to 18 °C and supplemented with 50 μM $FeCl_3$. After 30 minutes, protein expression was induced with the addition of 200 μM IPTG, and the cultures were allowed to incubate overnight.

Cell cultures were harvested by centrifugation and the pellet was resuspended in 25 mM HEPES at pH 7.5, 100 mM NaCl, 10 mM imidazole. The cells were lysed by sonication and the cleared lysate was passed through a Ni-NTA column pre-equilibrated with the above buffer maintained at 4 °C. The loaded column was then washed with 30 mM imidazole, and protein was eluted with 500 mM imidazole while collecting fractions. Fractions containing BesC were identified by SDS-PAGE (predicted MW = 29,700 Da). Pooled fractions were dialyzed against 3 L of working buffer (25 mM HEPES at pH 7.5, 100 mM NaCl, 10% glycerol) at 4 °C. Protein was concentrated using Millipore centrifugal filters (10K MWCO) and quantified by the absorbance at 280 nm using a calculated molar absorptivity of 34,400 M^{-1} cm^{-1}, and aliquots were flash frozen and stored at -80 °C until further use. Typical yields of BesC were ~200 mg protein/L bacterial culture. SDS-PAGE indicated a highly pure preparation (Fig. S1).

Expression and purification of BesD. The *besD* gene from *S. cattleya* was codon-optimized, synthesized, and subcloned into pET28b(+) with NdeI and HindIII restriction enzymes by Bio Basic for expression with an N-terminal hexahistidine tag. The final coding sequence follows:

ATGGGTTCTAACCGTCAGGAACTGAAAGACGTTTGCGCGCCGCTGGAAAAAGATGACATCCGTCGTCTGTCTCAGGC
GTTCCACCGTTTCGGTATCGTTACCGTTACCGAACTGATCGAACCGCACACTCGTAAACTGGTTCGTGCGGAAGCGG
ACCGTCTGCTGGATCAGTACGCAGAACGTCGTGACCTGCGTCTGGCTACCACCGACTACACCCGTCGTTCCATGTCT
GTTGTTCCGTCTGAAACCATCGCGGCTAACTCTGAACTGGTTACCGGTCTGTACGCACACCGTGAACTGCTGGCTCC
GCTGGAAGCAATCGCGGGTGAACGTCTGCACCCGTGCCCGAAAGCTGACGAAGAGTTCCTGATCACCCGTCAGGAAC
AGCGTGGTGATACCCACGGCTGGCACTGGGGTGACTTCTCTTTCGCGCTGATCTGGGTTCTGCAGGCTCCGCCGATC
GACGTTGGCGGCCTGCTGCAGTGCGTTCCGCACACCACCTGGGATAAAGCGAGCCCGCAGATCAACCGTTACCTGGT
TGAAAACCCGATCGACACCTACCACTTCGAATCTGGTGATGTTTACTTCCTGCGCACCGACACCACCCTGCACCGTA
CCATCCCGCTGCGTGAGGACACCACCCGTATCATCCTGAACATGACCTGGGCGGGTGAACGTGATCTGTCTCGTAAA
CTGGCGGCGGACGACCGTTGGTGGGACAACGCGGAAGTTTCTGCGGCGCGTGCGATCAAAGACTAA

Expression of BesD was carried out in an identical manner as described for BesC. Cell pellets were thawed and suspended in buffer (100 mM Tris, 10 mM imidazole, pH 7.60), lysed by sonication, and centrifuged at 20,000 rpm at 4 °C for 30 min. The supernatant was loaded onto a Ni-NTA column. The column was washed with ~ 3 column volumes of lysis buffer. The desired protein was then eluted using the elution buffer (100 mM Tris, 250 mM imidazole, pH 7.60). Fractions containing BesD were observed by SDS-PAGE and then concentrated using Millipore centrifugal filters (10K MWCO). The concentrated protein solution was dialyzed against Buffer A (100 mM Tris, 5 mM EDTA, pH 7.60) and then dialyzed twice against Buffer B (100 mM Tris, pH 7.60). Protein concentration was determined by the absorbance at 280 nm using a calculated molar absorptivity of 47,500 M^{-1} cm^{-1}. Typical yields of BesD were ~300 mg purified protein/L bacterial culture. SDS-PAGE indicated a highly pure preparation (Fig. S1).

Enzymatic preparation and purification of 4-Cl-L-lysine and d7-4-Cl-L-lysine. The 4-chloro-L-lysine (4-Cl-Lys) substrate was synthesized from L-lysine by the halogenase BesD.[1-2] A 5-mL reaction containing 0.2 mM BesD, 10 mM L-lysine, 20 mM alpha-ketoglutarate (αKG), 10 mM ascorbate, and 10 mM sodium chloride in 100 mM Tris buffer (pH 7.6) was allowed to incubate with shaking overnight (~14 hrs) at 220 rpm at 18 ˚C. Using these conditions, LC-MS indicated that all of the L-lysine was consumed, as confirmed by the characteristic isotopic ratio (^{35}Cl and ^{37}Cl) of the chlorinated product, which accounted for > 90% of the total metabolites (Fig. S2). The reaction was then quenched using an equal volume of acetonitrile. After centrifugation, the crude mixture was concentrated using a rotary evaporator. It was then dissolved in acetonitrile (1 mL) and immediately purified using HPLC on a Waters Xbridge Amide column (5 μm, 10 x 250 mm) using acetonitrile/10 mM ammonia acetate (63:37, vol:vol) as the eluent. The analytes were monitored at a wavelength of 205 nm. The combined fractions were collected and concentrated to give 4-Cl-Lys.The concentration of 4-Cl-Lys was determined by NMR using dioxane as an internal standard. For the reaction using 3,3,4,4,5,5,6,6-d_8-lysine as the substrate, both αKG and ascorbate were increased to 40 mM.

Selection of deuterated lysine. Two deuterated lysine isotopomers were investigated for reactivity with BesC, both perdeuterated (3,3,4,4,5,5,6,6-d_8 L-Lys) and tetradeuterated 4,4,5,5-d_4 L-Lys. Measurement of the reaction of BesC-P with either isotopomer resulted in the same slower decay rate compared to that of protiated L-Lys, which indicates BesC is reactive toward the same C–D bond in each case, rather than changing regiospecificity to favor the weaker C3–H or C6–H bonds of tetradeuterated L-Lys, a process termed "metabolic switching".[3] The identical behavior with each isotopologue reiterates the selectivity of BesC for C4–H abstraction as discussed in the Main Text. While this excludes the issue of metabolic switching for BesC, we nonetheless selected the perdeuterated d_8 L-Lys for preparation of deuterated 4-Cl-Lys by BesD because of the known consequences of metabolic switching in the αKG halogenase SyrB2 to compromise halogenase activity.[4]

NMR characterization of 4-Cl-L-lysine. The ^1H NMR spectrum of 4-Cl-L-lysine shows eight individual resonances (Fig. S3). Correspondingly, the ^{13}C and DEPT135 spectra display six carbon resonances with the presence of one carbonyl (δ_C 173.6), two methines (δ_C 55.9, 52.4), three methylenes (δ_C 38.8, 36.8, 35.1) (Figs. S4, S5). ^1H-^1H COSY spectra suggest a connective spin system of H-2/H-3/H-4/H-5/H-6 (Fig. S6). The corresponding HSQC spectrum is shown in Fig. S7. The HMBC correlation of H-2/C-1 and H-3/C-1

informs the C1-C2 connectivity (Fig. S8). In addition, the mass signal of 4-Cl-Lys corresponds to the calculated molecular ion peak of Cl-Lys. Taken together, the structure of the isolated BesD reaction product was confirmed as 4-Cl-Lys. The product of BesD with 3,3,4,4,5,5,6,6-d_8-Lys was also confirmed to be 3,3,4,5,5,6,6-d_7-4-Cl-Lys (d_7-4-Cl-Lys). The resonances of ^{1}H NMR (δ_H 3.99 (1H, s, at C2)) and ^{13}C NMR (δ_C 52.4(C-2)), 173.6(C-1)) resemble those observed for 4-Cl-lysine (Figs. S9, S10, S11).

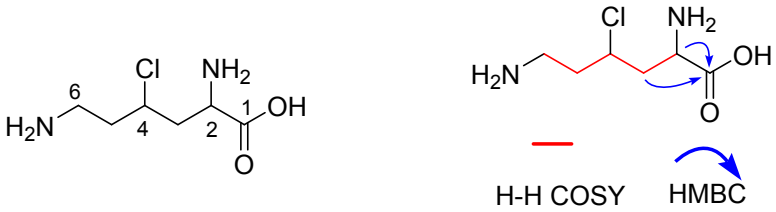

4-Cl-Lys: ^{1}H NMR (D_2O, 500 MHz) δ 4.17 (1H, tt, 10, 3.3, H-4), 3.99 (1H, dd, 9.2, 3.6, H-2), 3.26 (1H, m, H-6), 3.18 (1H, m, H-6), 2.38 (1H, m, H-3), 2.28 (1H, m, H-3), 2.21 (1H, m, H-5), 2.11 (1H, m, H-5); ^{13}C NMR (D_2O, 125 MHz) δ 173.6 (C-1), 55.9 (C-4), 52.4 (C-2), 38.8 (C-3), 36.8 (C-6), 35.1 (C-5).

d_7-4-Cl-Lys: ^{1}H NMR (D_2O, 500 MHz) δ 3.99 (1H, s, H-2); ^{13}C NMR (D_2O, 125 MHz) δ 173.6 (C-1), 52.3 (C-2).

Note on 4-Cl-Lys stability. In working with 4-Cl-Lys, we observed small amounts of the hydroxylated byproduct 4-hydroxy-L-lysine (4-OH-Lys) even after purification by LC-MS. Previous work demonstrates that not only can OH-Lys be produced as a side-product in the BesD reaction, but it also forms due to the non-enzymatic hydrolysis of the chloro group over time.[1] We have observed that 4-Cl-Lys can be maintained through storage at -20 °C or by handling on ice and using within 6 h. Nonetheless, some minor 4-OH-Lys content is inevitable. Thus, as a control, we sought to generate pure 4-OH-Lys to react with BesC. By heating 4-Cl-Lys to 65 °C for 5 min, virtually all of the 4-Cl-Lys was converted to 4-OH-Lys as confirmed by LC-MS (Fig. S22). The reactivity of BesC was assessed by stopped-flow (Fig. S23) and it was found that 4-OH-Lys triggers BesC-P poorly and results in a very slow decay of BesC-P. Additionally, analysis of single- and multiple-turnover reactions with 4-Cl-Lys and some 4-OH-Lys present showed that 4-OH-Lys was not depleted. Thus, the small amounts of this byproduct do not have a significant influence on the observed reactivity of BesC-P with 4-Cl-Lys.

Reconstitution of BesC. Apo-BesC was made anaerobic by successive evacuations and refills with inert gas via Schlenk line. The putative diiron cluster was reconstituted by the addition of 2 mol. equiv. of ferrous ammonium sulfate from an anaerobic stock solution. The reconstitution was allowed to incubate for several minutes. The protein was then ready for use. For experiments in which BesC was reacted with substrate or substrate analogs, the substrate was included with the protein prior to degassing.

UV-visible spectroscopy. Absorption spectra were measured using an Agilent Cary 60 UV-visible spectrophotometer. The spectra were measured at protein concentrations of 100-300 μM. Spectra of reconstituted ferrous BesC were measured in a sealed, anaerobic cuvette. The sample was then exposed to O_2. Time-course measurements were used to examine the decay of BesC-P with L-Lys and d_8-L-Lys.

Mössbauer spectroscopy. BesC was prepared for Mössbauer spectroscopy by concentrating to ~1 mM and reconstituting with 2 mol. equiv. of ferrous ammonium sulfate as described above. For preparation of the substrate-bound form and the oxygenated intermediate, 5 mol. equiv. of L-Lys or purified 4-Cl-Lys was added to the protein prior to reconstitution. To prepare the oxygenated intermediate species, the reconstituted samples were evacuated and refilled with O_2 gas while stirring at 4 °C. Samples were transferred to Delrin Mössbauer cups and frozen in liquid nitrogen for storage until further use. Spectra were collected with home-built spectrometers using Janis Research Super-Varitemp dewars, which allowed studies in the temperature range from 1.5 to 200 K and applied magnetic fields up to 8.0 T. Mössbauer

spectral simulations were performed using the WMOSS software package (SEE Co., Edina, MN). Isomer shifts are quoted relative to Fe metal at 298 K. All Mössbauer figures were prepared using SpinCount software.[5]

The following spin Hamiltonian was used to generate the spectral simulations included in Figure S20:

$$\hat{H} = J\boldsymbol{S_1}\cdot\boldsymbol{S_2} + \sum_{i=1,2}\{g_0\beta\boldsymbol{S_i}\cdot\boldsymbol{B} + \boldsymbol{S_i}\cdot\boldsymbol{D_i}\cdot\boldsymbol{S_i} + A_0\boldsymbol{S_i}\cdot\boldsymbol{I_i} - g_n\beta_n\boldsymbol{I_i}\cdot\boldsymbol{B}\}$$

where i = 1,2 sums over the two ferric sites with $S_1 = S_2 = 5/2$. The zero-field splittings of the high-spin ferric sites in non-heme iron enzymes are generally small, $D_i < 2$ cm^{-1}, and can be ignored. The g tensor for high-spin ferric centers is generally isotropic and can be estimated as an isotropic value of $g_0 = 2$. The ^{57}Fe hyperfine coupling tensor ($\boldsymbol{A}$) for high-spin ferric center is rather isotropic and can be estimated with an isotropic value of $A_0/g_n\beta_n = -21$ T. For the current case, $J > 0$, which suggests that the two ferric center is antiferromagnetically coupled to yield an $S = 0$ ground spin state with the $S = 1$ state as the first excited state of the spin-coupled system. By measuring Mössbauer spectrum at an elevated temperature, such as 50 K used in this study, the $S = 1$ excited state will be thermally populated if J is not large. For $J = 35$ cm^{-1}, the energy gap between the $S = 0$ and the $S = 1$ states is 35 cm^{-1}, which is equivalent to ~ 50 K. Thus, at 50 K, the $S = 1$ state is thermally populated. The thermal population of the $S = 1$ state will be reflected by the internal field (B_{int}) sensed by the ^{57}Fe nuclei. Thus, the spectral simulation of the 50 K spectrum could provide a good estimation of J. A similar type of analysis has been used to analyze many spin-coupled diferric species, in particular for peroxo-diferric species.[6-8] The simulation parameters used are: g values for both ferric sites were kept at $g_0 = 2$, A values for both ferric sites were kept at $A_0/g_n\beta_n = -21$ T, $D_1 = D_2 = 1$ cm^{-1}, $J = 35$ cm^{-1}, $\Delta E_{Q1} = \Delta E_{Q2} = 1.15$ mm/s, $\eta_1 = \eta_2 = 1$, $\delta_1 = \delta_2 = 0.57$ mm/s.

Turnover of BesC and LC-MS analysis. For single-turnover reactions, a 400-μL reaction containing 100 μM BesC, 250 μM substrate (L-Lys, 4-Cl-Lys, or their deuterated forms) and 250 μM of a glycine internal standard in buffer (25 mM HEPES pH 7.5, 100 mM NaCl) was evacuated and refilled with nitrogen gas via Schlenk line. Ferrous ammonium sulfate (200 μM from an anaerobic stock solution prepared in the same buffer) was added. The solution was then uncapped and O_2 was blown over the solution while stirring. After 15 min, reactions were quenched by the addition of an equal volume of acetonitrile. The precipitated protein was then pelleted by centrifugation and the resulting supernatant was analyzed by LC-MS as described below. Multiple turnover reactions of BesC were carried out by combining a solution containing 50 μM BesC, 500 μM of the desired substrate, 100 μM ferrous ammonium sulfate, 5 mM ascorbate, and 250 μM glycine internal standard with an equal volume of O_2-saturated buffer. The reactions were left stirring at room temperature and quenched at the desired time point (1 h unless otherwise stated) as described above.

For product analysis, a 1-μL aliquot was injected onto an LC-MS equipped with an Agilent Poroshell 120 HILIC column (2.7μm, 4.6 x 50 mm), followed by isocratic elution with 60% acetonitrile/H_2O (0.1% formic acid). The reaction was monitored using Agilent 6120 Quadrupole mass spectrometer under electrospray ionization in positive mode (ESI^+). The associated Agilent MassHunter and OpenLAB software package were used for data collection and analysis. The LC-MS chromatograms shown were collected using selective ion monitoring mode of the proton ion adduct ($[M+H]^+$).

^{18}Oxygen isotopic tracer studies. Isotopic labeling experiments were performed on single turnovers with L-Lys as described above. For experiments with $^{18}O_2$, the reaction vial was evacuated, kept sealed, and then refilled with $^{18}O_2$ gas (99% ^{18}O) while stirring. For the reaction in $H_2{}^{18}O$, the buffer was prepared by drying a specified volume of buffer in a speed-vac and re-dissolving in ^{18}O-water (97% ^{18}O). The reaction solution was then prepared from concentrated stocks of BesC, substrate, iron, and internal standard such that the volume added did not exceed 5% of the total reaction volume, providing a final > 90% enrichment of the reaction mixture with ^{18}O-water.

Transient kinetics studies. Stopped-flow spectroscopy was performed on an Applied Photophysics SX20 spectrophotometer equipped with a photodiode array detector for collection of full spectral data or a photomultiplier tube for measurement of single-wavelength data. Time-dependent data was collected using a logarithmic time-base. All experiments were performed in 25 mM HEPES at pH 7.5, 100 mM NaCl at 4 °C. General reactions of BesC with various substrates were performed by mixing an anaerobic solution of BesC, 2 mol. equiv. ferrous ammonium sulfate, and at least 3 mol. equiv. of the desired substrate against a solution of O_2-saturated buffer. O_2 titrations were performed by combining O_2-saturated buffer with different amounts of anaerobic buffer immediately before loading onto the stopped-flow. Substrate titrations were performed by adding different quantities of substrate to BesC prior to degassing the solution.

Fitting of single-wavelength data was performed using Pro-Data software. Kinetic traces at 612 nm of the reaction of BesC and 4-Cl-Lys with O_2 were fit to a two-summed ($n = 2$) exponential expression as listed below, where $A_{t,\,obs}$ is the observed absorbance, A_{max} is the maximum absorbance, a_i is the amplitude of phase i, $1/t_i$ is the reciprocal relaxation time (per second), and t is time in seconds. Traces at 612 nm of BesC with L-Lys reacting with O_2 required fitting with a three-summed ($n = 3$) exponential expression.

$$A_{t,\,obs} = A_{max} + \sum_{i=1}^{n} a_i\, e^{-t/t_i}$$

Assignment of reciprocal relaxation times. The two reciprocal relaxation times (RRTs) measured for the 612-nm timecourses of BesC and 4-Cl-Lys in the reaction O_2 were examined by varying the oxygen concentration and the nature of the substrate under pseudo-first order conditions in O_2. It was revealed that only the fast RRT ($1/t_1$= 1.6 ± 0.3 s^{-1}) displayed a dependence on oxygen concentration (Fig. 1C) thus it can be attributed to the formation of the diferric-peroxo intermediate. The slower RRT ($1/t_2$ = 0.030 ± 0.001 s^{-1}) was O_2-independent (Fig. S11) but sensitive to substrate deuteration and thus can be ascribed to the rate of the diferric-peroxo-mediated C–H (or C-D) cleavage step.

In contrast to the two phases at 612 nm observed for BesC with 4-Cl-Lys, BesC with L-Lys displayed three phases. Of the three RRTs determined from fitting these phases, two of the RRTs corresponded to formation phases (negative spectral amplitude) and the third represented a decay process (positive amplitude). As observed for 4-Cl-Lys, only the slowest RRT ($1/t_3$ = 0.00064 ± 0.00007) was affected by substrate deuteration and again can be ascribed to the rate of peroxo-mediated C–H scission.

Of the two formation phases, both had very similar spectral amplitudes, but only the faster phase ($1/t_1$) showed a dependence on the concentration of oxygen (Fig. S12) and, thus, can be assigned to the oxygen-binding step. The fit in Fig. S12B shows a near but non-zero intercept. This would appear to imply that O_2-binding in the presence of L-Lys is reversible. However, we note the inherent difficulty in obtaining absolute oxygen concentrations, which could affect the reliability of this value. Therefore we cannot definitely conclude whether O_2-binding is reversible from analysis of $1/t_1$ alone, but analysis of the other RRTs shed some light.

If the oxygen binding step represented by $1/t_1$ is reversible and is the first step in the sequence, then the plots of the RRTs of one of the following steps ($1/t_2$ or $1/t_3$) vs [O_2] should show a hyperbolic dependence on [O_2], which are not observed. If the oxygen binding step is irreversible, then the following reciprocal relaxation times would be anticipated to be O_2-independent, as is shown in Fig. S12C. Thus, the non-zero y-intercept of the ($1/t_1$) vs. O_2 plot may be artificial. However, an alternative rationale for the [O_2]-independence of $1/t_2$ is that it precedes the step represented by $1/t_1$ (i.e., $1/t_2$ represents the first step in

sequence). Both kinetic models (irreversible O_2 binding and/or $1/t_2$ representing the first step) satisfy the kinetic observations.

Analysis of C–H abstraction rates by BesC-P. Determination of the rate of C–H abstraction by BesC-**P** is complicated in the cases of d_7-4-Cl-Lys, L-Lys, and d_8-L-Lys due to varying degrees of uncoupling of peroxo decay from productive catalysis. In the case of 4-Cl-Lys, BesC-**P** is fully coupled (1 mol. equiv. substrate consumed per peroxo in single-turnover reactions), thus the rate of BesC-**P** decay of 0.030 s^{-1} can be exclusively attributed to C–H scission. However, with d_7-4-Cl-Lys, BesC-**P** decay bifurcates into two routes: C–D abstraction and non-productive decay in roughly equal measures. The aggregate rate observed for BesC-**P** decay is 0.011 s^{-1}. From this, the relative amounts of the products (in this case 50/50%) can be used to delineate the magnitudes of the individual rates of each process by the following relationship: $[\text{4-Cl-Lys}]_{\text{final}} = [\text{4-Cl-Lys}]_{\text{initial}} \times k_{\text{C–D}}/(k_{\text{C–D}} + k_{\text{uncoupling}})$ where $k_{\text{C–D}} + k_{\text{uncoupling}} = k_{\text{obs}}$. We refer interested readers to an excellent discussion from Pan *et al*.[9] As such, we estimate a rate of $k_{\text{C–D}}$ at 0.0055 s^{-1} (Table S7), giving rise to an estimate of the ^{2}H-KIE ~ 5, and still below the semi-classical threshold for tunneling.

As for the reactivity of BesC-**P** toward L-Lys, and d_8-L-Lys, uncoupling is observed with both of these substrates. Thus, there is uncertainty in the rate of C–H(D) scission in each case. Considering that single turnover reactions with L-Lys demonstrate 50/50% metabolism/uncoupling, we can again use this ratio to estimate the true rate of C–H abstraction from L-Lys as 0.00034 s^{-1}. However, since BesC-**P** decay with d_8-L-Lys exhibits nearly full uncoupling, we cannot determine the true rate of C–D scission with this substrate. Thus, the apparent ^{2}H-KIE of (d_8-) L-Lys of 2.7 has significant uncertainty.

Supplementary Figures

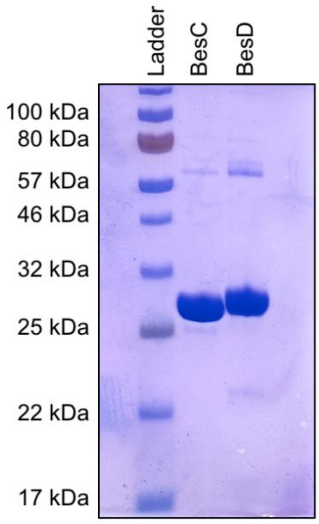

Figure S1: Representative SDS-PAGE of purified BesC and BesD. Predicted molecular weights are 29.7 and 29.0 kDa, respectively.

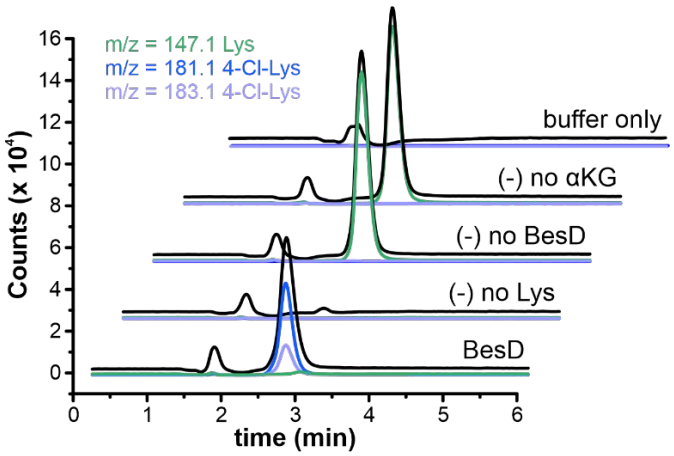

Figure S2: Analysis of the multiple turnover reaction performed by BesD by liquid chromatography-mass spectrometry. The total ion chromatogram is shown in black, and the extracted ion chromatograms for the substrate L-Lys and product 4-Cl-Lys and are shown in the designated colors. Reported are representative chromatograms from at least three experimental replicates.

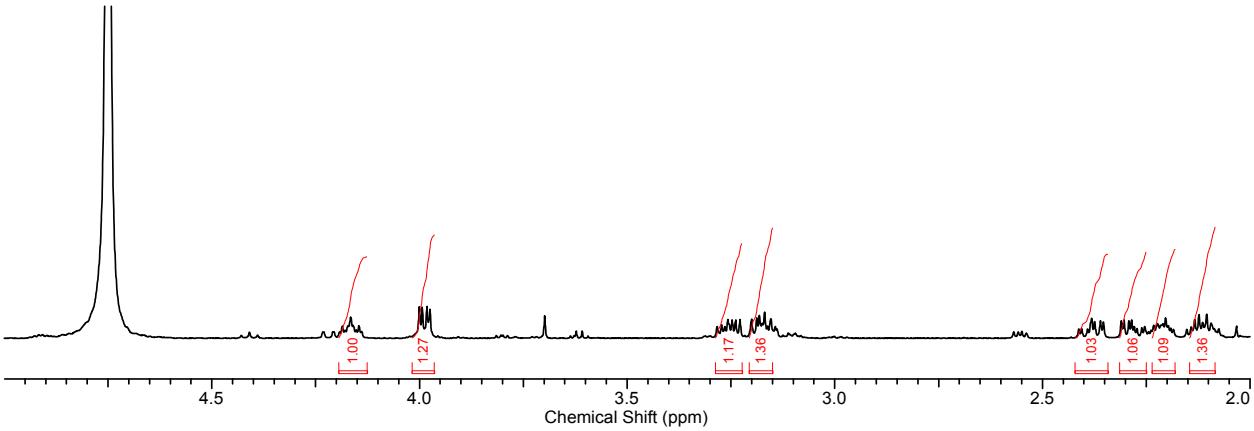

Figure S3: ^{1}H NMR spectrum of 4-Cl-lysine purified from the reaction of BesD with L-Lys.

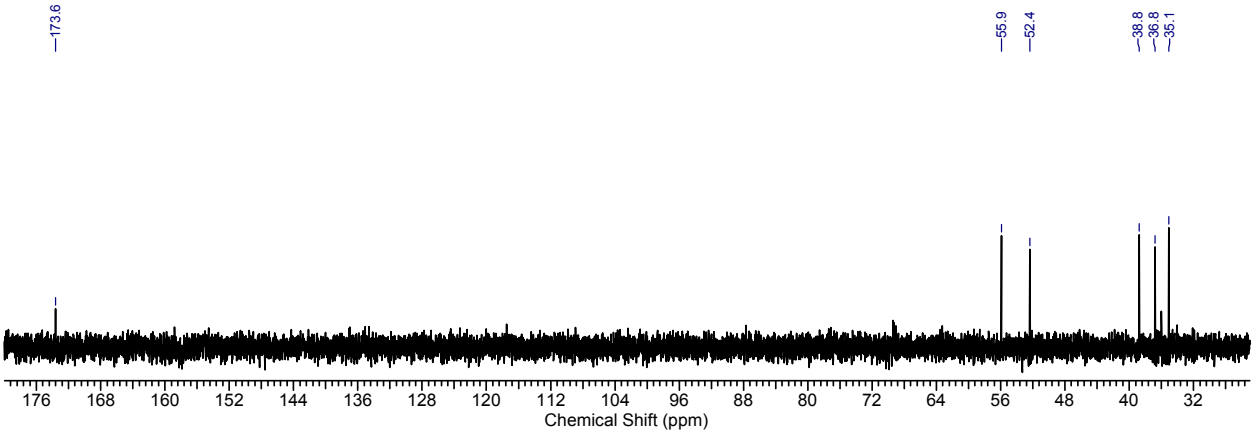

Figure S4: ^{13}C NMR spectrum of 4-Cl-Lys purified from the reaction of BesD with L-Lys.

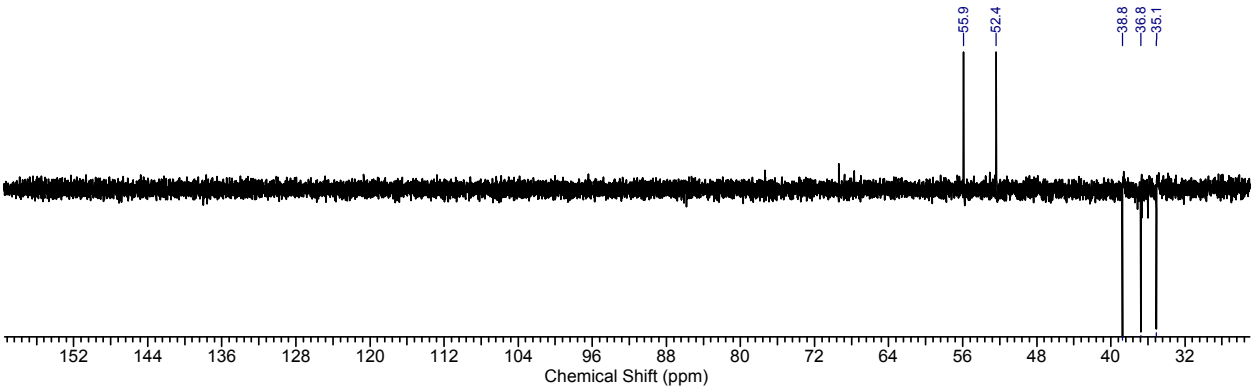

Figure S5: DEPT135 spectrum of 4-Cl-Lys purified from the reaction of BesD with L-Lys.

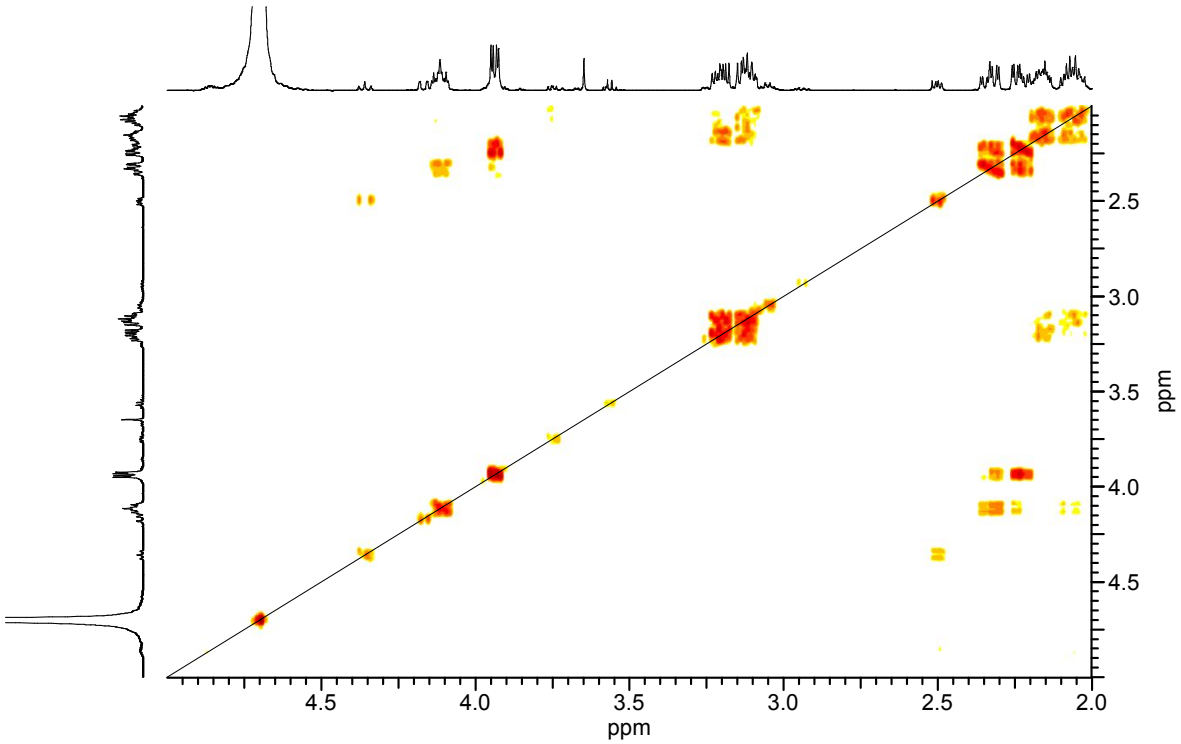

Figure S6: ^{1}H-^{1}H COSY of 4-Cl-Lys purified from the reaction of BesD with L-Lys.

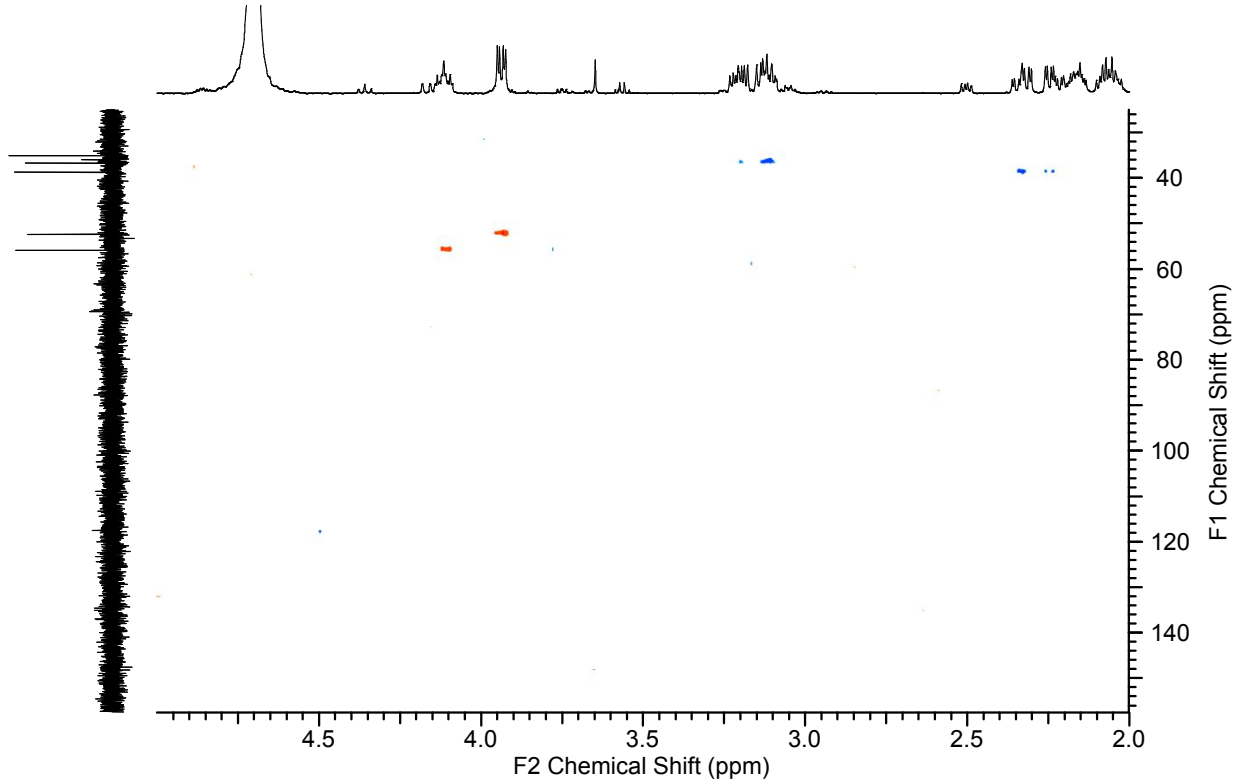

Figure S7: HSQC of 4-Cl-Lys purified from the reaction of BesD with L-Lys.

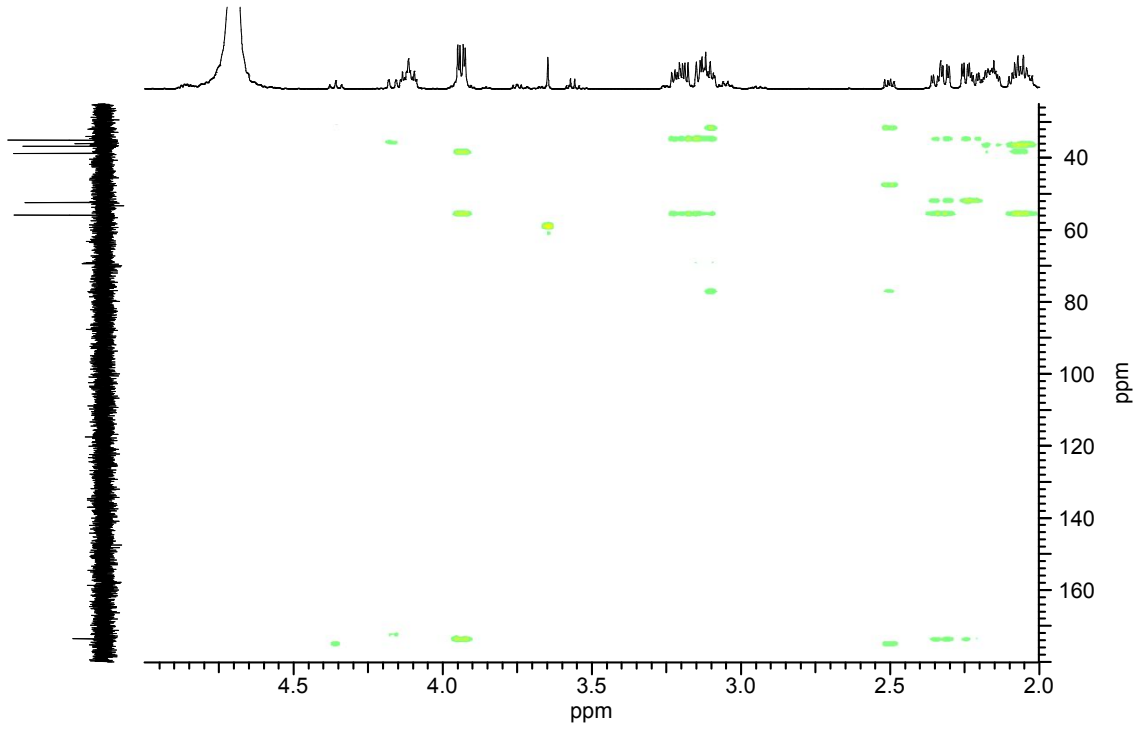

Figure S8: HMBC spectrum of 4-Cl-Lys.

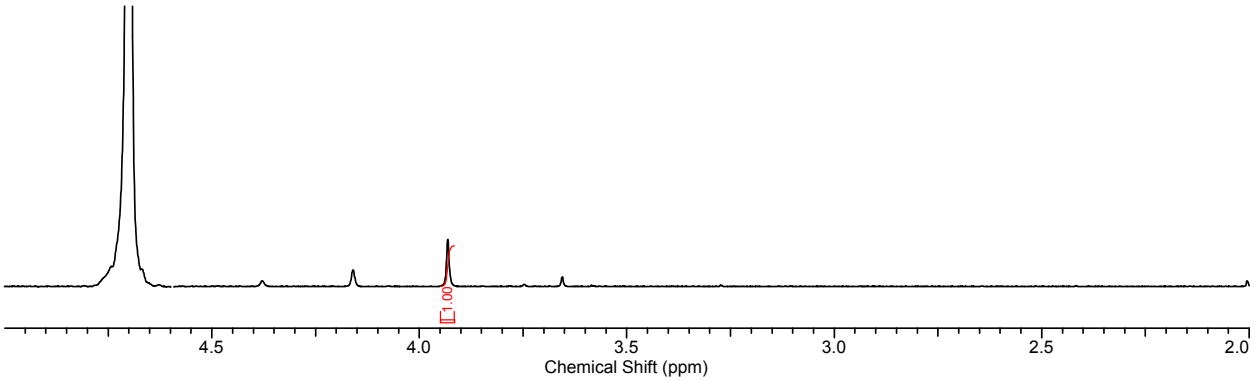

Figure S9: ^{1}H NMR spectrum of 3,3,4,5,5,6,6-d$_7$-4-Cl-Lys purified from the reaction of BesD with 3,3,4,4,5,5,6,6-d$_8$-L-Lys.

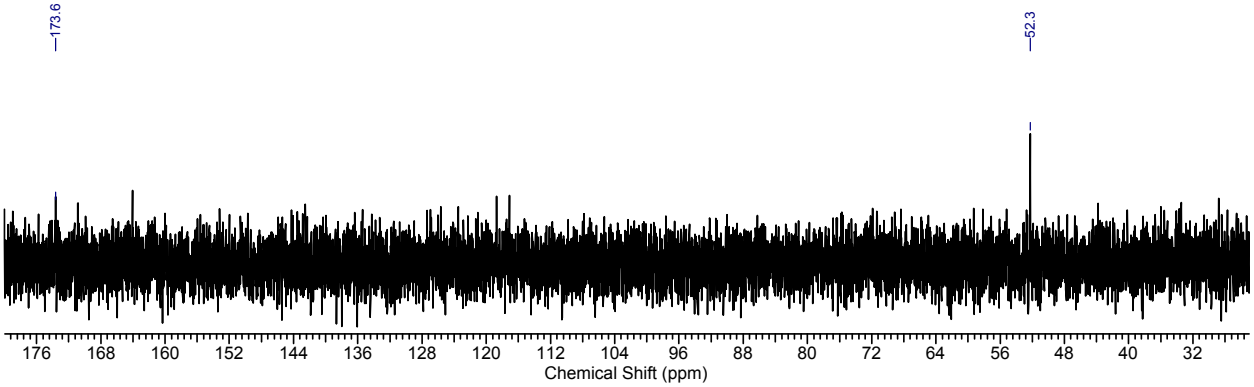

Figure S10: ^{13}C NMR spectrum of 3,3,4,5,5,6,6-d$_7$-4-Cl-Lys purified from the reaction of BesD with 3,3,4,4,5,5,6,6-d$_8$ L-Lys.

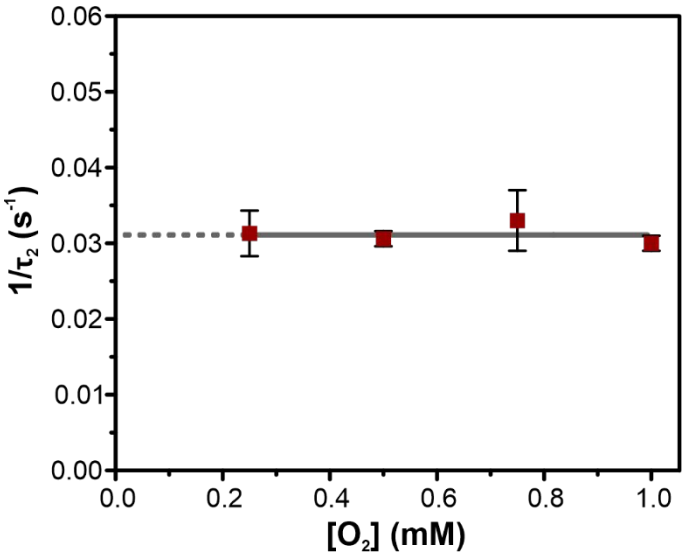

Figure S11: Measurement of the second reciprocal relaxation time ($1/t_2$) corresponding to BesC-P decay versus O_2 concentration in the reaction of BesC + 4-Cl-Lys with O_2 at 4 °C.

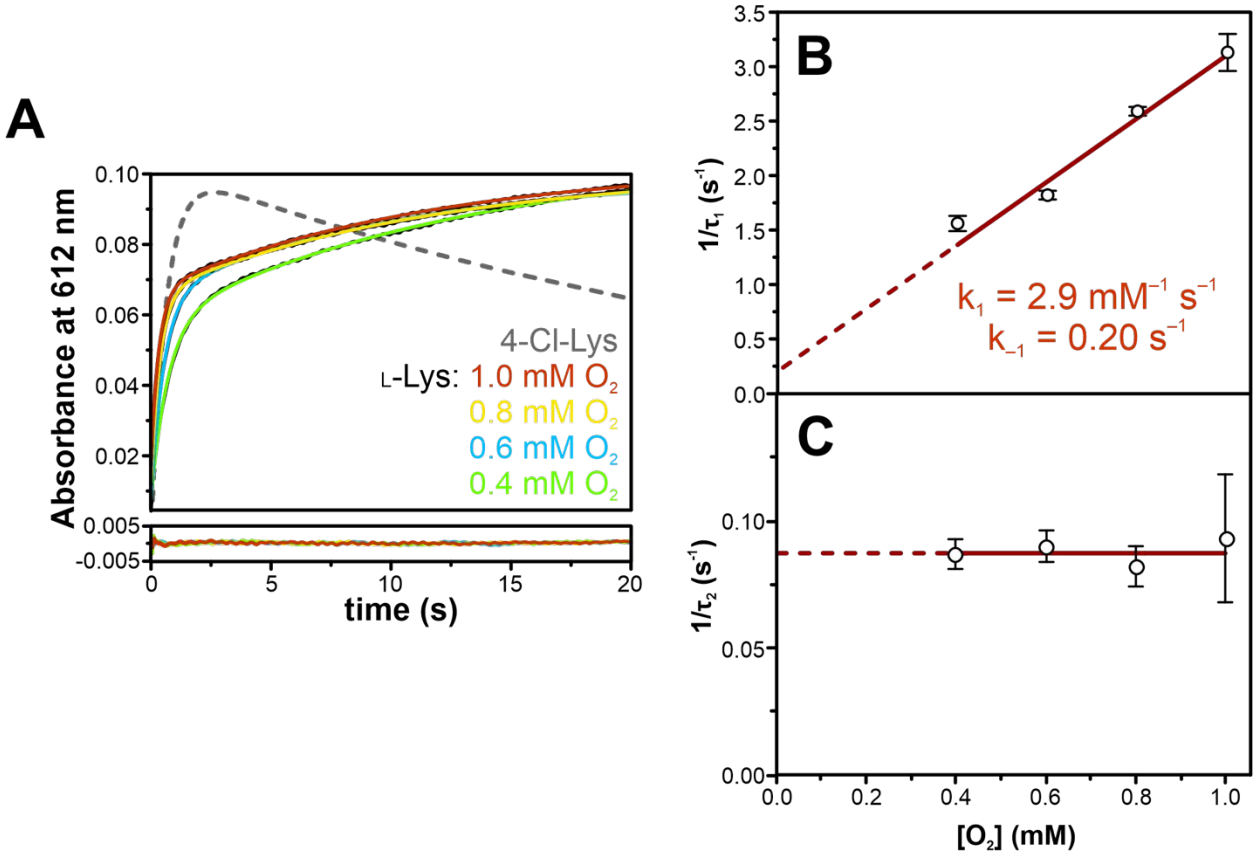

Figure S12: Triggering of O_2 activation by L-Lys. A. The reaction of L-Lys-bound BesC with varying concentrations of O_2 as monitored by the absorbance at 612 nm by photomultiplier tube on a stopped-flow spectrophotometer at 4 °C. The raw data is shown in black with the fit with a two-exponential expression is shown in the designated color. The 612-nm trace of BesC with 4-Cl-Lys showing faster formation (and decay) is shown in a gray dashed line. Decay of BesC-P + L-Lys occurs on a longer time-scale, shown in Fig. 4B. **B.** For the reaction of the reaction of diferrous BesC + L-Lys with O_2, dependence of the first reciprocal relaxation time versus O_2 concentration can be fit with a line with a non-zero *y*-intercept. **C.** The second reciprocal relaxation time in unaffected by $[O_2]$.

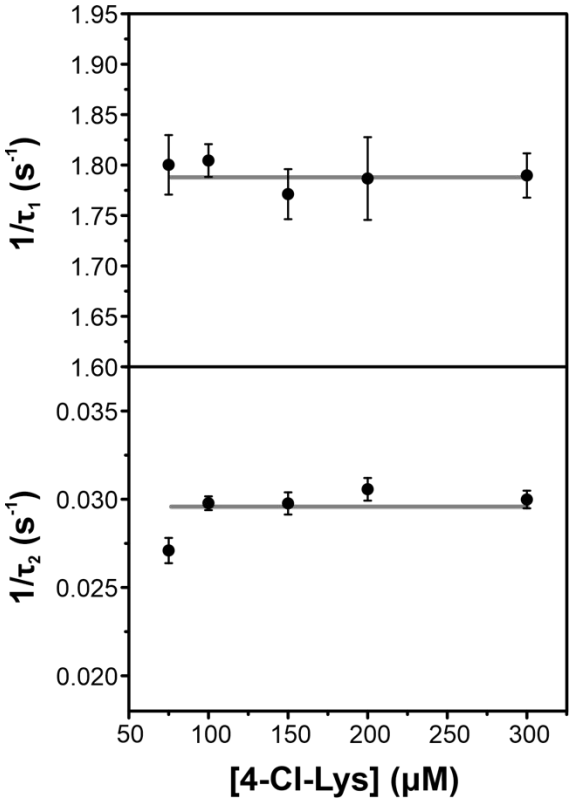

Figure S13: The formation (top) and decay (bottom) phases of BesC-P with 4-Cl-Lys are independent of the concentration of 4-Cl-Lys, as determined from stopped-flow kinetics at 4 °C.

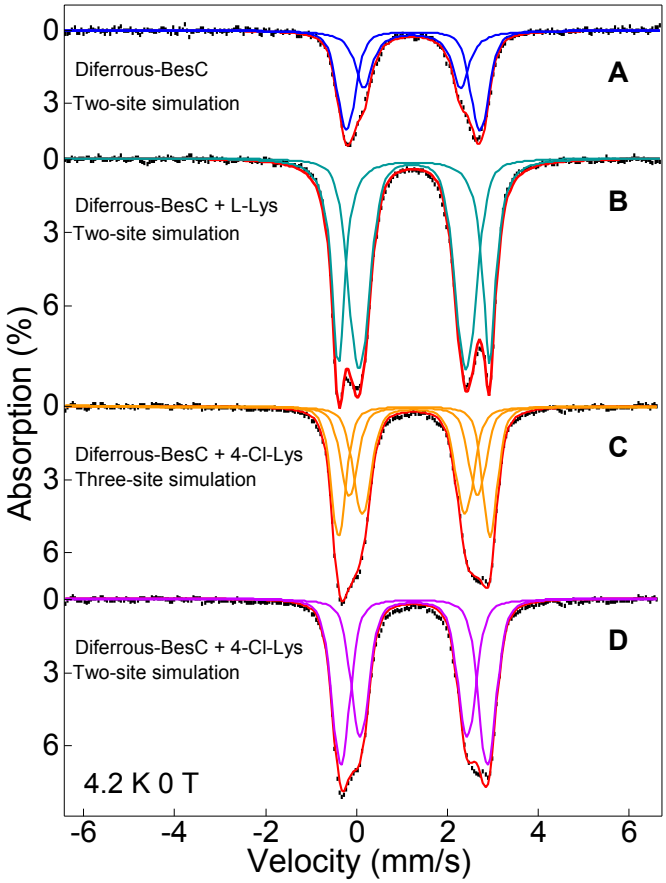

Figure S14: 4.2 K zero-field Mössbauer spectra (black vertical bars) of ferrous BesC (**A**), Lys-bound (**B**), and 4-Cl-Lys-bound BesC (**C** and **D**) and the associated overall spectral simulations (red solid lines) and the sub spectral components (solid lines with various colors). All the simulation parameters are listed in Table 1 and Table S2.

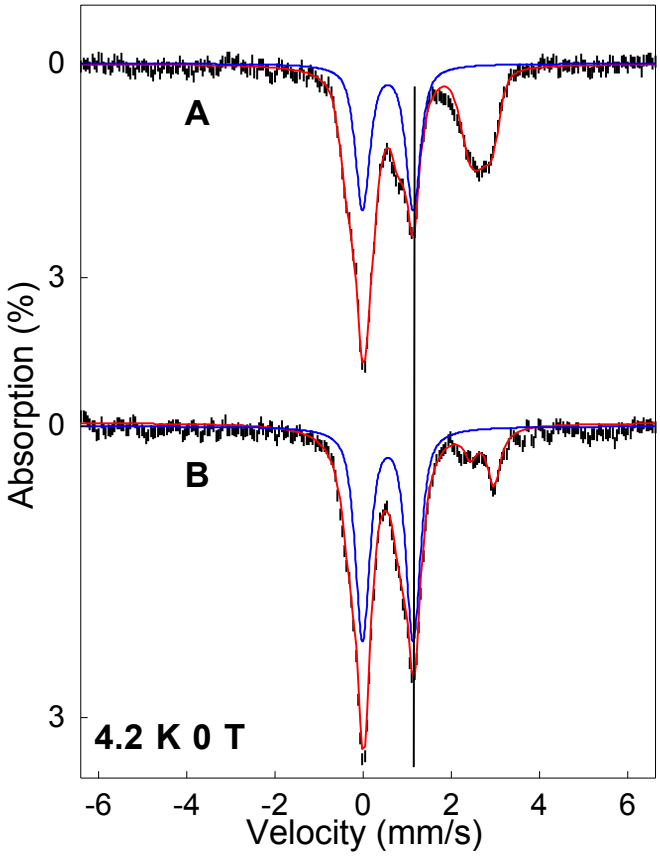

Figure S15: Comparison of the 4.2 K zero field Mössbauer spectra of BesC-P prepared with 4-Cl-Lys and Lys. (**A**) The Mössbauer spectrum (black) and the overall simulation (red) of the BesC reaction with 4-Cl-Lys; (**B**) The Mössbauer spectrum (black) and the overall simulation (red) of the BesC reaction with L-Lys. The blue lines are spectral simulations of BesC-P found in the two spectra. The vertical line indicates the high-energy absorption line of BesC-P.

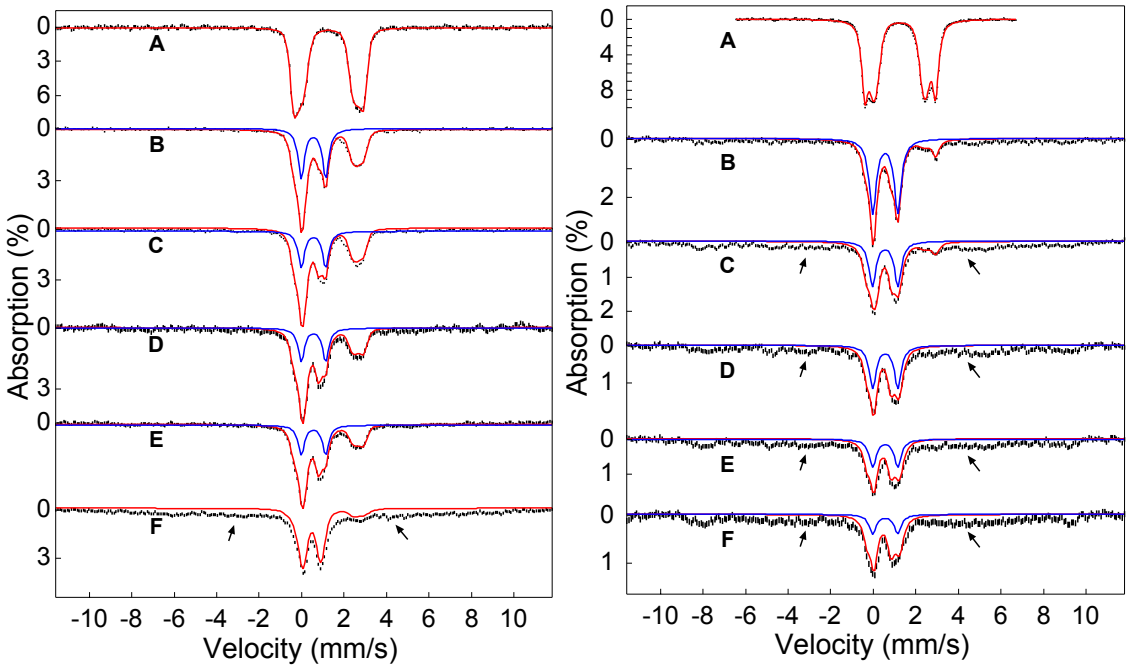

Figure S16: 4.2 K zero field Mössbauer spectra of the time-course of the decay of BesC-P with 4-Cl-Lys and L-Lys. Left: (**A**) 4-Cl-Lys-bound diferrous BesC; (**B**) Oxygenated 4-Cl-Lys-bound diferrous BesC frozen at shortest time; (**C**) Oxygenated 4-Cl-Lys-bound diferrous BesC frozen at 1 minute; (**D**) Oxygenated 4-Cl-Lys-bound diferrous BesC frozen at 2 minutes; (**E**) Oxygenated 4-Cl-Lys-bound diferrous BesC frozen at 3 minutes; (**F**) Oxygenated 4-Cl-Lys-bound diferrous BesC frozen at 20 minutes. Right: (**A**) L-Lys-bound diferrous BesC; (**B**) Oxygenated L-Lys-bound diferrous BesC frozen at shortest time; (**C**) Oxygenated L-Lys-bound diferrous BesC frozen at 10 minutes; (**D**) Oxygenated L-Lys-bound diferrous BesC frozen at 20 minutes; (**E**) Oxygenated L-Lys-bound diferrous BesC frozen at 40 minutes; (**F**) Oxygenated L-Lys-bound diferrous BesC frozen at 60 minutes. The red solid lines are the overall spectral simulations, the blue lines represent the spectral component of BesC-P. The black arrows indicate the spectral features representing the mononuclear ferric species accumulated at longer reaction times.

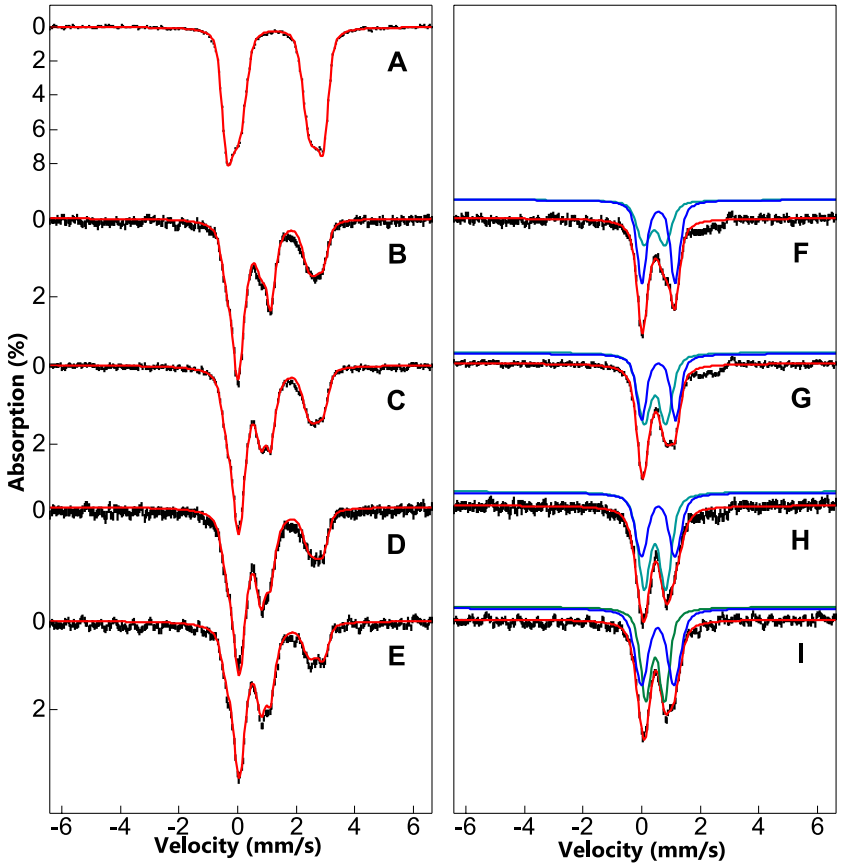

Figure S17: 4.2-K, zero-field Mössbauer spectra of the time course demonstrating the interconversion of BesC-P with the initial product complex in the BesC reaction with 4-Cl-Lys. (**A**) 4-Cl-Lys-bound diferrous BesC; (**B**) Oxygenated 4-Cl-Lys-bound diferrous BesC frozen at shortest time; (**C**) Oxygenated 4-Cl-Lys-bound diferrous BesC frozen at 1 minute; (**D**) Oxygenated 4-Cl-Lys-bound diferrous BesC frozen at 2 minutes; (**E**) Oxygenated 4-Cl-Lys-bound diferrous BesC frozen at 3 minutes; (**F**) The difference spectrum generated by (**B**)-40%(**A**); (**G**) the different spectrum generated by (**C**)-40%(**A**); (**H**) the different spectrum generated by (**D**)-35%(**A**); (**I**) the different spectrum generated by (**E**)-30%(**A**). The red solid lines are the overall spectral simulation. The blue solid lines represent the spectral component of BesC-P. The green solid lines represent the spectral component of the initial product complex.

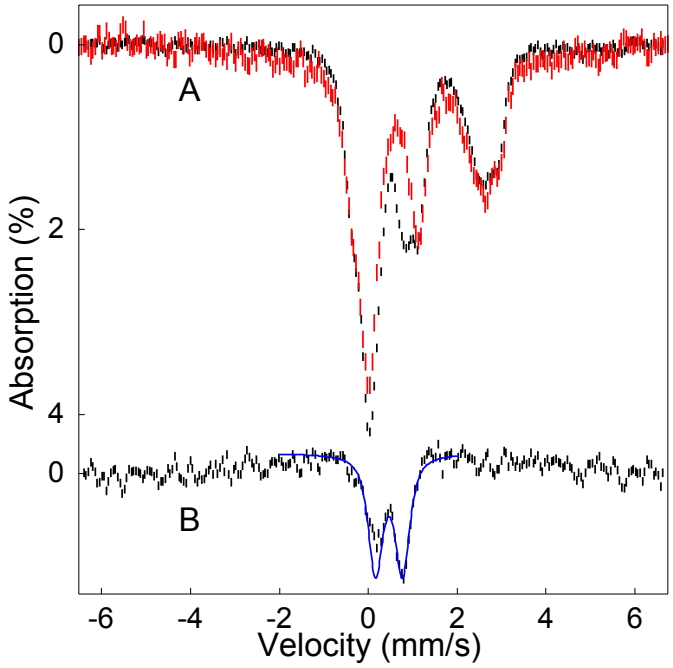

Figure S18: 4.2 K Mössbauer spectra demonstrating the magnetization behavior of the initial product complex Species II. (**A**) The spectra of oxygenated 4-Cl-Lys-bound diferrous BesC frozen at 1 minute measured at zero field (black) and under 0.45 mT applied field parallel to the gamma radiation (red); (**B**) the difference spectrum generated by substrating the zero field spectrum from the the 0.45 mT field spectrum. The blue solid line represents the quadrupole doublet simulation of the initial product complex.

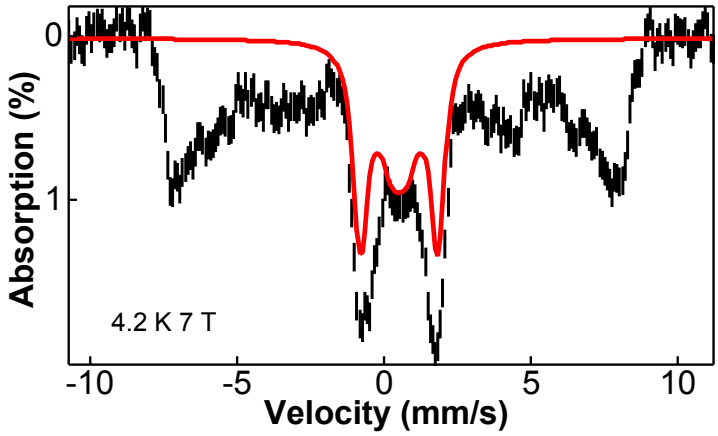

Figure S19: 4.2 K high-field Mössbauer spectra of the decayed BesC-P. The red line represents the simulation for a diferric species with parameters δ = 0.50 mm/s, ΔE_Q = 0.82 mm/s, Γ = 0.5 mm/s, which represents ~ 40% of the total iron in the sample. The rest of the absorption (~60%) belong to high-spin mononuclear ferric species.

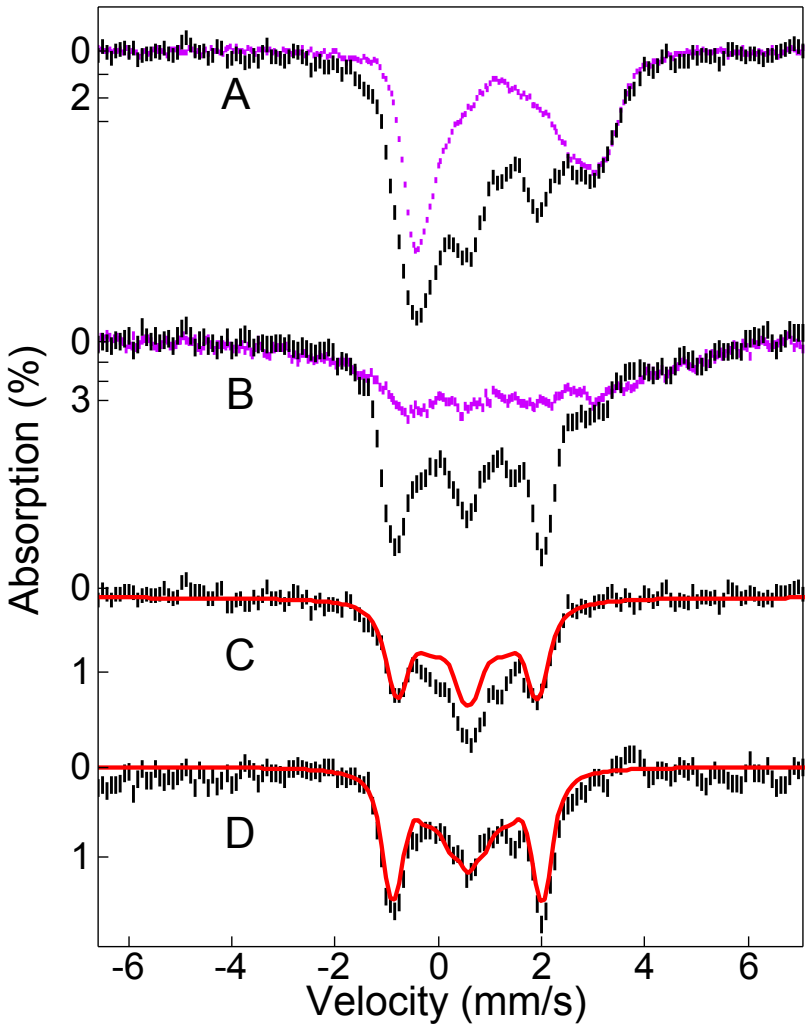

Figure S20. Mössbauer spectra used to determine the exchange coupling constant for BesC-P. The Mössbauer spectra of the 4-Cl-Lys-bound diferrous BesC (purple) and the oxygenated 4-Cl-Lys-bound diferrous BesC frozen at shortest time (black) measured at 50 K (A) and 4.2 K (B) with 7 T applied magnetic field parallel to the gamma radiations. The purple spectra are drawn to 40% of the area relative to the black spectra to match with the diferrous components in the black spectra. The difference spectrum of the black spectrum – the purple spectrum in (A) and (B) are shown in (C) and (D) respectively. The red solid lines are spectral simulation using an exchange coupling constant $J = 35$ cm^{-1} (in the convention defined by the Hamiltonian $H = J\boldsymbol{S_1} \cdot \boldsymbol{S_2}$, see the Mössbauer spectroscopy section of the SI for more details on the spectral simulation).

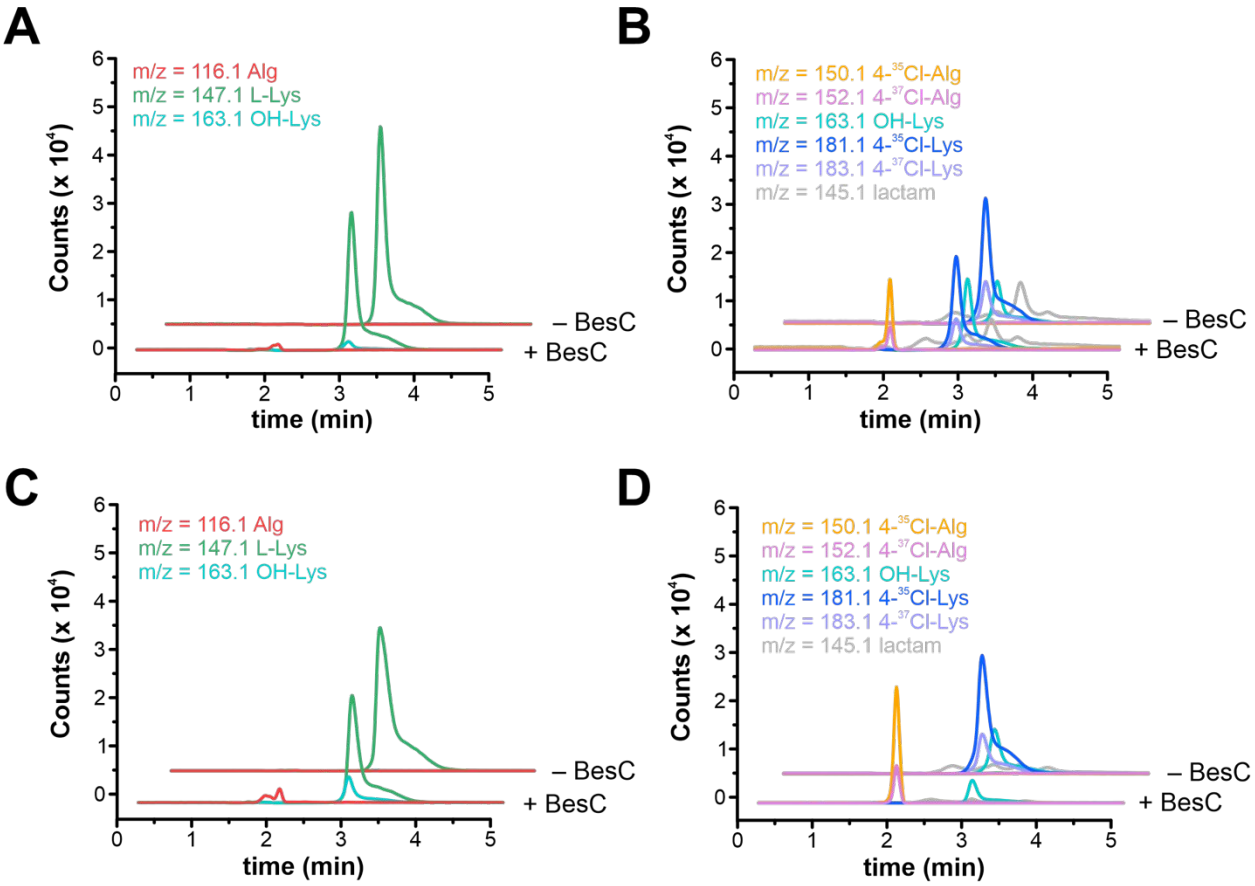

Figure S21: Representative LCMS extracted ion chromatograms showing single turnover reactions of BesC with L-Lys (**A**) and 4-Cl-Lys (**B**) and multiple turnover reactions (t = 1 h) of BesC with L-Lys (**C**) and 4-Cl-Lys (**D**), and a no-BesC negative control (– BesC) of each. Shown are representative chromatograms from at least three experimental replicates.

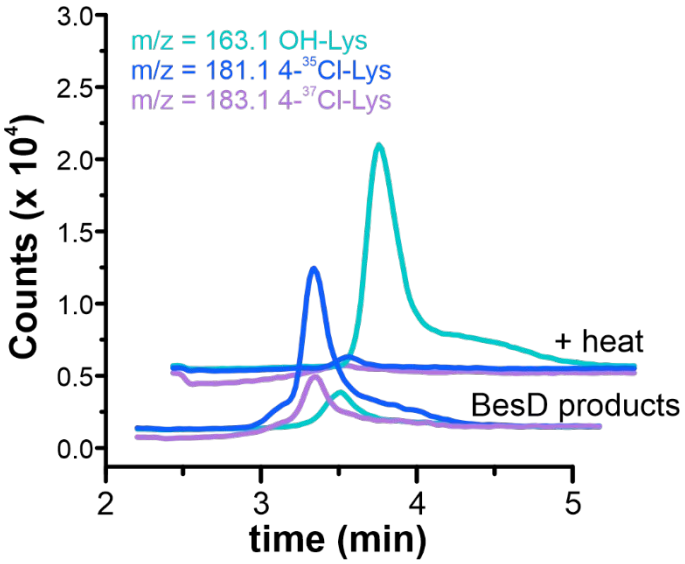

Figure S22: Extracted ion chromatograms of the reaction products of BesC before (bottom) and after (top) heating at 65 °C for 5 minutes.

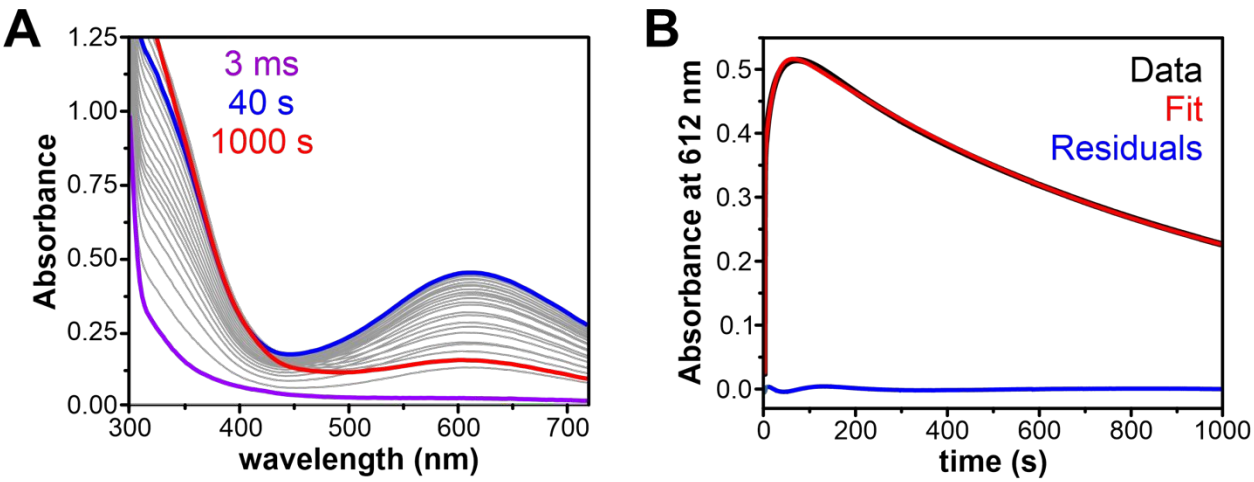

Figure S23: A. Photodiode array spectra of the reaction of diferrous BesC with 4-OH-Lys rapidly mixed with O_2-saturated buffer. **B.** Single-wavelength trace monitoring the formation and decay of BesC-P in the presence of 4-OH-Lys. Raw data is shown in black and the fit and residuals in red and blue, respectively.

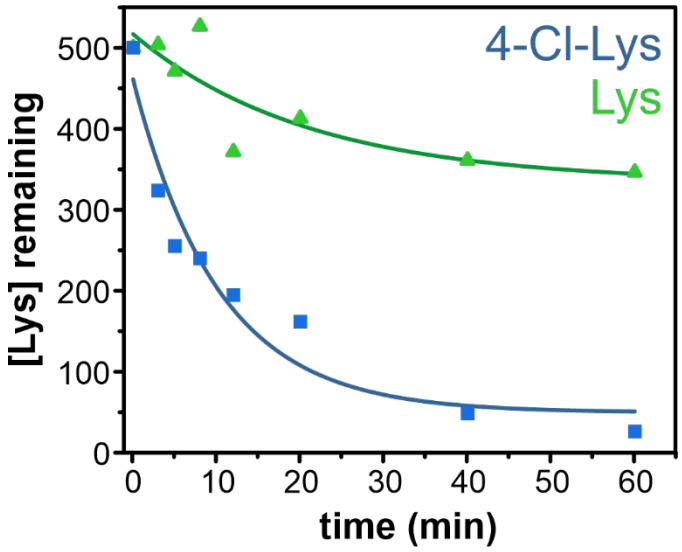

Figure S24: The time-course of substrate (L-Lys or 4-Cl-Lys) remaining during a multiple turnover reaction containing 100 μM BesC, 500 μM substrate, 200 μM ferrous ammonium sulfate, and 2.5 mM ascorbate. Rate of substrate consumption was ~21 min^{-1} for Cl-Lys and ~10 min^{-1} min for L-Lys.

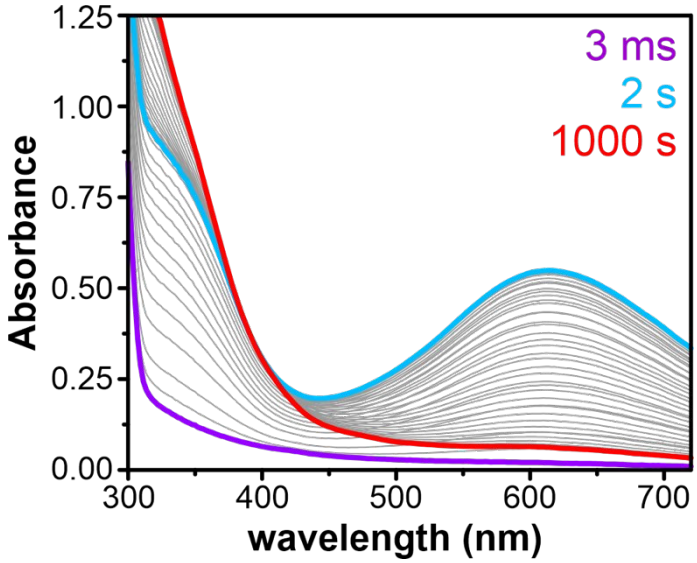

Figure S25: The PDA spectra of 300 µM BesC + 5 mol. equiv. of d_7-4-Cl-Lys mixed with O_2-saturated buffer at 4 °C. Single-wavelength data data is shown in Fig. 4C.

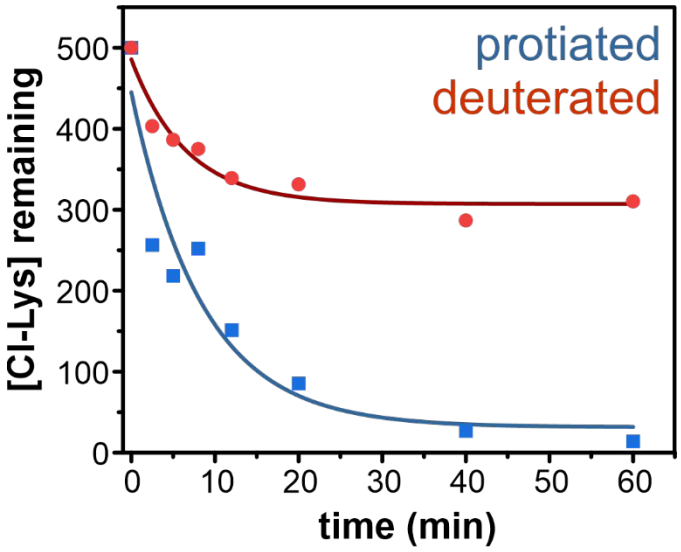

Figure S26: A time-course of substrate (protiated 4-Cl-Lys or perdeuterated d_7-4-Cl-Lys) remaining during a multiple turnover reaction containing 100 μM BesC, 500 μM substrate, 200 μM ferrous ammonium sulfate, and 2.5 mM ascorbate. The ratio of protiated vs. deuterated substrate metabolized of ~2.5, which is reflective of the ^{2}H-KIE.

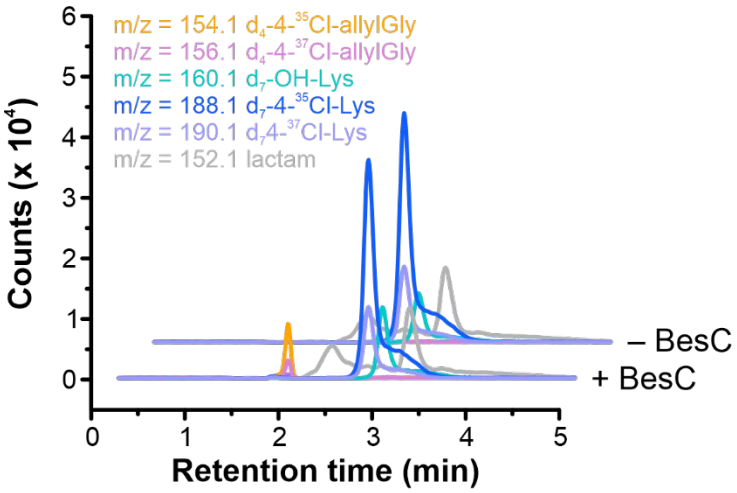

Figure S27: Representative extracted ion chromatograms showing a single turnover reaction of BesC with deuterated 4-Cl-Lys (d_7-4-Cl-Lys) and a no-BesC negative control (– BesC).

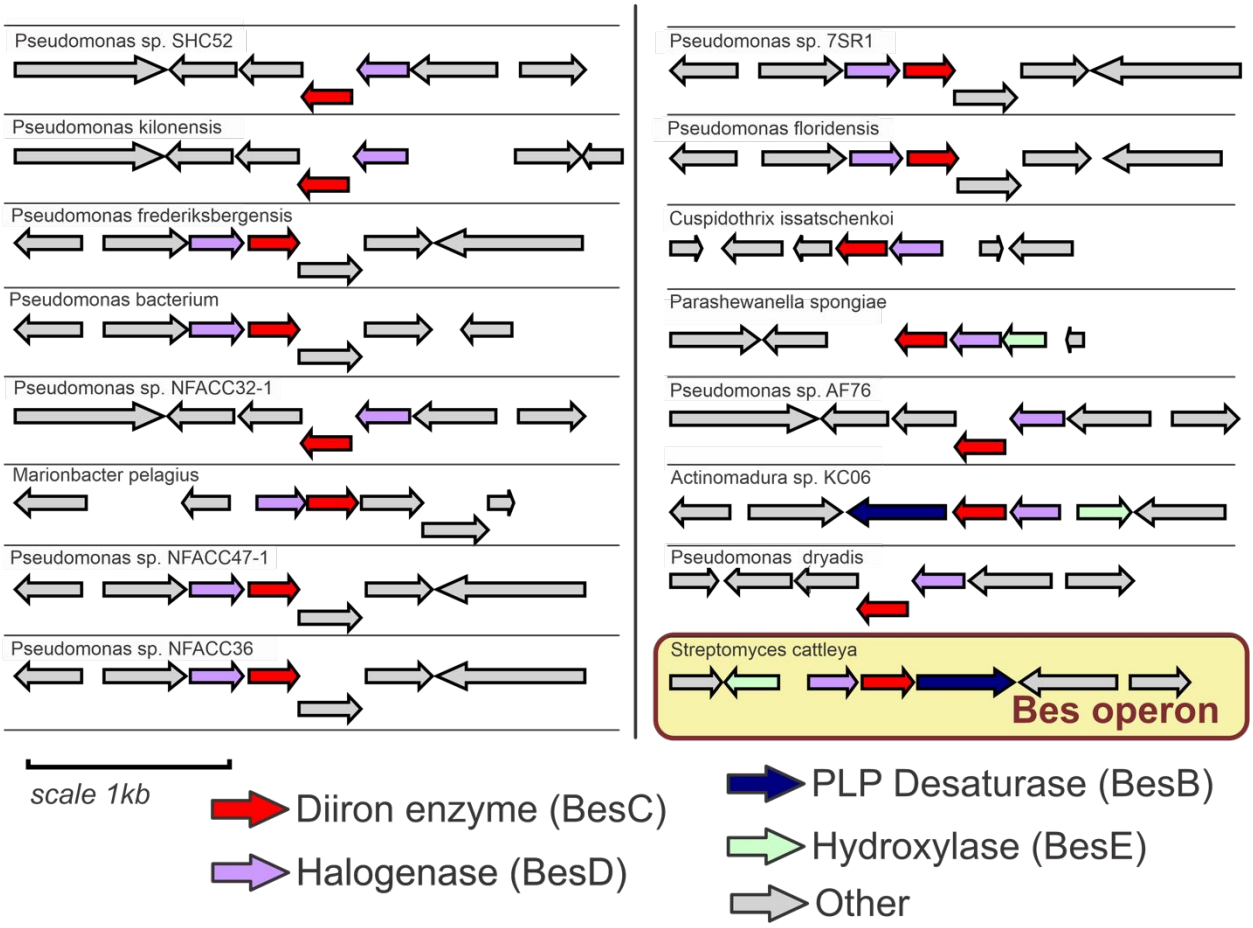

Figure S28: Bioinformatic analysis of gene clusters containing BesC orthologs. A sequence similarity network was generated using an alignment score of 40 and the genomic neighborhood was manually examined using the Genome neighborhood tool.[10] BesC, BesD, and BesB orthologs are shown in red, purple, and blue respectively.

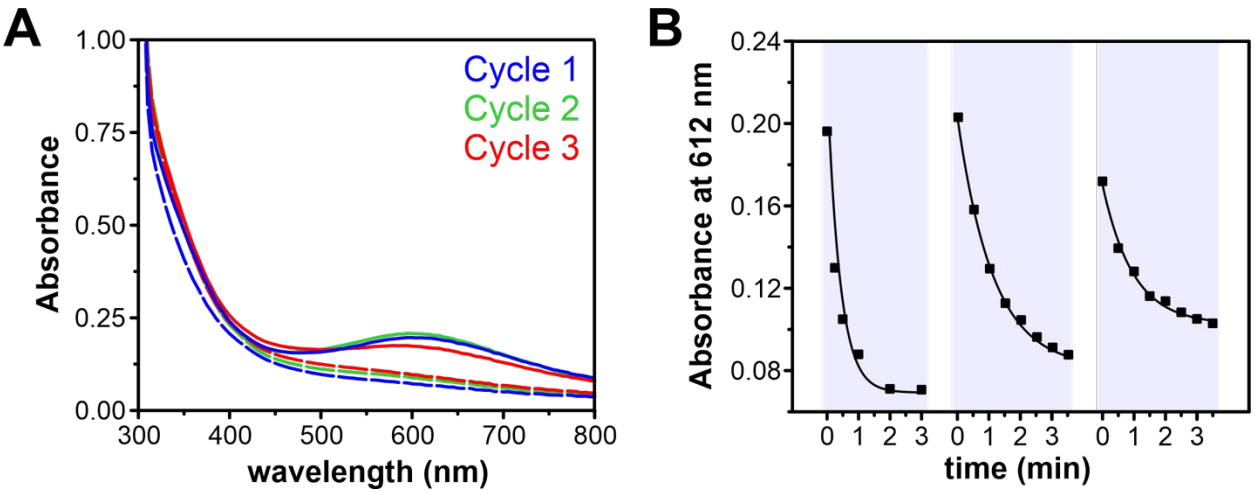

Figure S29: Recycling of BesC-P at room temperature. A. The absorption spectra of maximum accumulation of BesC-P (solid lines) and the fully decayed diferric state (dashed lines) upon multiple rounds of oxygen activation. **B.** The time course of the BesC-P decay. Each cycle of reduction and oxygenation is denoted by a break in the shaded region. It is unclear whether the decrease in total absorption over multiple cycles is related to an inability to fully re-form an intact cluster or is caused by the experimental conditions, considering that some protein was lost to aggregation during the multiple rounds of degassing, reducing, and reoxygenating.

Table S1: Catalytic diferric-peroxo intermediates in diiron enzymes.

Enzyme	λ (nm)	ε (M^{-1} cm^{-1})	δ [ΔE_Q] (mm/s)	ν(O–O) [^{18}O shift] (cm^{-1})	Assignment	Refs.
MMO	725	2000	0.66 [1.51]	n.d.	(μ-1,2-peroxo)[a]	11-12
Δ^9D	700	1200	0.64 [1.06], 0.68 [1.90]	898 [-54]	μ-1,2-peroxo	13-14
$RNR_{W48X/D84E}$	700[a]	1500[a]	0.60 [1.47], 0.66 [1.68][b]	870 [-46][c]	μ-1,2-peroxo	15-16
ToMOH	n.a.	n.a.	0.55 [0.67]	n.d.	(μ-1,1-(hydro)peroxo)[a]	17
DOHH	630	2800	0.55 [1.16], 0.58 [0.88]	855 [-44]	μ-1,2-peroxo	8, 18
CmlI/AurF	500	500	0.54 [-0.68], 0.62 [-0.23]	791 [-43]	μ-1,1-(hydro)peroxo	7, 19
UndA	550	1600	0.59 [1.07], 0.56 [0.67]	n.d.	n.d.	20
SznF	629	3100	0.60 [1.00]	n.d.	(μ-1,2-peroxo)[a]	21
BesC	**612**	**2300**	**0.56 [1.2]**	**n.d.**	**n.d.**	***This work***

[a]Assignment is not definitive because of a lack of direct structural information available.
[b]X = A, [c]X = F

Table S2: Mossbauer parameters of alternative fitting of diferrous BesC shown in Fig. S14D.

	Site	δ (mm/s)	ΔE_Q (mm/s)	Γ (mm/s)	Spectral area (%)
Diferrous + 4-Cl-Lys	1	1.28	3.23	-0.45	53
	2	1.26	2.36	-0.45	46

Table S3: Mössbauer parameters of BesC with L-lysine.

	Site	δ (mm/s)	ΔE_Q (mm/s)	Γ (mm/s)	Spectral area (%)
Diferrous + L-Lys	1	1.27	3.33	0.35	45
	2	1.24	2.35	-0.55	55
BesC-P + L-Lys	1	0.57	1.18	0.40	51
Diferric (decayed BesC-P)	1	0.48	0.80	0.43	29
	2	0.50	1.54	0.40	17

Table S4: Mössbauer parameters of the diferrous states of asymmetrically coordinated diiron proteins substrate-free and substrate-bound (if available).

Enzyme	State	δ (mm/s)	[ΔE_Q] (mm/s)	Relative area (%)	Substrate-triggered?	Refs.
SznF	Diferrous	1.2	3.0	n.a.[a]	No	[22]
CmlI	Diferrous	1.25 1.23	3.13 2.80	n.d.[b]	No	[7]
AurF	Diferrous	1.24	3.06	n.a.[a]	No	[23-24]
	+intermediate *p*-nitrosobenzoate	1.23	3.00	n.a.[a]		
UndA	Diferrous	1.25 1.23	2.93 1.87	48 52	Yes	[25]
	+substrate lauric acid	1.26 1.24	3.01 2.05	65 35		
BesC	**Diferrous**	**1.25** **1.24**	**2.97** **2.15**	**60** **40**	**Yes**	***This work***
	+substrate 4-Cl-L-lysine	**1.28** **1.26** **1.26**	**3.34** **2.83** **2.26**	**37** **28** **35**		
	+substrate L-lysine	**1.27** **1.25**	**3.33** **2.38**	**52** **48**		

[a]n.a. = not applicable

[b]n.d. = no data

Table S5. Simulation parameters of Mössbauer spectra of the samples in the reaction time course of 4-Cl-Lys bound diferrous-BesC with O_2 in Figure S16 (left).*

Site	Ferrous 1	Ferrous 2	Ferrous 3	BesC-P	Initial Product (Species II)	Final Diferric
δ (mm/s)	1.26	1.28	1.26	0.56	0.46	0.49
ΔE_Q (mm/s)	2.26	3.34	2.83	1.15	0.68	0.87
Γ (mm/s)	-0.45	-0.34	-0.42	0.36	0.45	0.50
Percentage for each site in different samples						
Starting 4-Cl-Lys complex	35	36	28	0	0	0
+O_2, frozen immediately (t = 0)	16	13	13	33	18	0
+O_2, t = 1 min	15	11	11	24	27	0
+O_2, t = 2 min	14	12	8	22	36	0
+O_2, t = 3 min	10	10	7	20	34	0
+O_2, t = 20 min	2	2	2	0	0	45

* The percentage for each species was determined by the zero field Mössbauer spectra measured under a large velocity scale (± 10 mm/s).

Table S6. Simulation parameters of Mössbauer spectra of the samples in the reaction time course of L-Lys bound diferrous-BesC with O_2 in Figure S16 (right).*

Site	Ferrous 1	Ferrous 2	BesC-P	Final Diferric I	Final Diferric II
δ(mm/s)	1.24	1.27	0.57	0.48	0.50
ΔE_Q(mm/s)	2.35	3.33	1.18	0.80	1.54
Γ(mm/s)	-0.55	0.35	0.40	0.43	0.40
Percentage for each site in different samples					
Starting L-Lys Complex	55	45	0	0	0
+O_2, frozen immediately (t = 0)	4	10	51	17	0
+O_2, t = 10 min	2	4	21	24	10
+O_2, t = 20 min	0	0	14	27	16
+O_2, t = 40 min	0	0	8	24	15
+O_2, t = 60 min	0	0	7	29	17

* The percentage for each species was determined by the zero field Mössbauer spectra measured under a large velocity scale (± 10 mm/s).

Table S7: The observed BesC-P formation and decay rates, their amplitudes, and the corresponding rate of C–H cleavage when accounting for uncoupling.

	Amp.	$k_{form\ 1}$ (s^{-1})	Amp.	$k_{form\ 2}$ (s^{-1})	Amp.	k_{decay} (s^{-1})	$k_{C–H}$ (s^{-1})
L-Lys	-33%	1.7 ± 0.2	-18%	0.11 ± 0.06	49%	0.00064 ± 0.00007	0.00034 ± 0.0003
3,3,4,4,5,5,6,6-d_8-L-Lys	-30%	2.4 ± 0.2	-16%	0.23 ±	55%	0.00027 ± 0.00004	n.a.
4-Cl-L-Lys	-51%	1.6 ± 0.3	n.a.	n.a.	49%	0.030 ± 0.001	0.030 ± 0.001
3,3,4,5,5,6,6-d_7-4-Cl-L-Lys	-59%	1.7 ± 0.1	n.a.	n.a.	41%	0.011 ± 0.001	0.0055 ± 0.0005
4-OH-L-Lys	-34%	2.3 ± 0.1	-17%	0.05 ± 0.01	49%	0.0011 ± 0.0001	n.a.

n.a. = not applicable

Table S8: Putative substrate analogs and their ability to trigger the formation of BesC-P.

Trigger	Do not trigger
L-lysine	L-glutamic acid
D-lysine	L-glutamine
L-ornithine	L-alanine
L-arginine	6-aminocaproic acid
L-norleucine	

References

1. Marchand, J.; Neugebauer, M.; Ing, M.; Lin, C.-I.; Pelton, J.; Chang, M., Discovery of a pathway for terminal-alkyne amino acid biosynthesis. *Nature* **2019,** *567* (7748), 420-424.
2. Neugebauer, M. E.; Sumida, K. H.; Pelton, J. G.; McMurry, J. L.; Marchand, J. A.; Chang, M. C., A family of radical halogenases for the engineering of amino-acid-based products. *Nature chemical biology* **2019,** *15* (10), 1009-1016.
3. Atkins, W. M.; Sligar, S. G., Metabolic switching in cyctochrome P-450cam: deuterium isotope effects on regiospecificity and the monooxygenase/oxidase ratio. *Journal of the American Chemical Society* **1987,** *109* (12), 3754-3760.
4. Matthews, M. L.; Neumann, C. S.; Miles, L. A.; Grove, T. L.; Booker, S. J.; Krebs, C.; Walsh, C. T.; Bollinger, J. M., Substrate positioning controls the partition between halogenation and hydroxylation in the aliphatic halogenase, SyrB2. *Proceedings of the National Academy of Sciences* **2009,** *106* (42), 17723-17728.
5. Petasis, D. T.; Hendrich, M. P., Quantitative Interpretation of Multifrequency Multimode EPR Spectra of Metal Containing Proteins, Enzymes, and Biomimetic Complexes. *Method Enzymol* **2015,** *563*, 171-208.
6. Krebs, C.; Bollinger, J. M., Jr.; Theil, E. C.; Huynh, B. H., Exchange coupling constant J of peroxodiferric reaction intermediates determined by Mossbauer spectroscopy. *J Biol Inorg Chem* **2002,** *7* (7-8), 863-9.
7. Grant, J. L.; Hsieh, C. H.; Makris, T. M., Decarboxylation of fatty acids to terminal alkenes by cytochrome P450 compound I. *Journal of the American Chemical Society* **2015,** *137* (15), 4940-4943.
8. Vu, V. V.; Emerson, J. P.; Martinho, M.; Kim, Y. S.; Münck, E.; Park, M. H.; Que, L., Human deoxyhypusine hydroxylase, an enzyme involved in regulating cell growth, activates O2 with a nonheme diiron center. *Proceedings of the National Academy of Sciences* **2009,** *106* (35), 14814-14819.
9. Pan, J.; Wenger, E. S.; Matthews, M. L.; Pollock, C. J.; Bhardwaj, M.; Kim, A. J.; Allen, B. D.; Grossman, R. B.; Krebs, C.; Bollinger Jr, J. M., Evidence for modulation of oxygen rebound rate in control of outcome by iron(II)-and 2-oxoglutarate-dependent oxygenases. *Journal of the American Chemical Society* **2019,** *141* (38), 15153-15165.
10. Gerlt, J. A., Genomic Enzymology: Web Tools for Leveraging Protein Family Sequence-Function Space and Genome Context to Discover Novel Functions. *Biochemistry-Us* **2017,** *56* (33), 4293-4308.
11. Liu, K. E.; Valentine, A. M.; Qiu, D.; Edmondson, D. E.; Appelman, E. H.; Spiro, T. G.; Lippard, S. J., Characterization of a diiron (III) peroxide intermediate in the reaction cycle of methane monooxygenase hydroxylase from Methylococcus capsulatus (Bath). *Journal of the American Chemical Society* **1995,** *117* (17), 4997-4998.
12. Liu, K. E.; Wang, D.; Huynh, B. H.; Edmondson, D. E.; Salifoglou, A.; Lippard, S. J., Spectroscopic detection of intermediates in the reaction of dioxygen with the reduced methane monooxygenase/hydroxylase from Methylococcus capsulatus (Bath). *Journal of the American Chemical Society* **1994,** *116* (16), 7465-7466.
13. Broadwater, J. A.; Ai, J.; Loehr, T. M.; Sanders-Loehr, J.; Fox, B. G., Peroxodiferric intermediate of stearoyl-acyl carrier protein Δ9 desaturase: oxidase reactivity during single turnover and implications for the mechanism of desaturation. *Biochemistry* **1998,** *37* (42), 14664-14671.
14. Broadwater, J. A.; Achim, C.; Münck, E.; Fox, B. G., Mössbauer studies of the formation and reactivity of a quasi-stable peroxo intermediate of stearoyl-acyl carrier protein Δ^9-desaturase. *Biochemistry* **1999,** *38* (38), 12197-12204.
15. Bollinger, J. M.; Krebs, C.; Vicol, A.; Chen, S.; Ley, B. A.; Edmondson, D. E.; Huynh, B. H., Engineering the diiron site of Escherichia coli ribonucleotide reductase protein R2 to accumulate an intermediate similar to H_{peroxo}, the putative peroxodiiron (III) complex from the methane monooxygenase catalytic cycle. *Journal of the American Chemical Society* **1998,** *120* (5), 1094-1095.

16. Moënne-Loccoz, P.; Baldwin, J.; Ley, B. A.; Loehr, T. M.; Bollinger, J. M., O2 activation by non-heme diiron proteins: identification of a symmetric μ-1,2-peroxide in a mutant of ribonucleotide reductase. *Biochemistry* **1998,** *37* (42), 14659-14663.
17. Murray, L. J.; Naik, S. G.; Ortillo, D. O.; García-Serres, R.; Lee, J. K.; Huynh, B. H.; Lippard, S. J., Characterization of the arene-oxidizing intermediate in ToMOH as a diiron(III) species. *Journal of the American Chemical Society* **2007,** *129* (46), 14500-14510.
18. Han, Z.; Sakai, N.; Böttger, L. H.; Klinke, S.; Hauber, J.; Trautwein, A. X.; Hilgenfeld, R., Crystal structure of the peroxo-diiron (III) intermediate of deoxyhypusine hydroxylase, an oxygenase involved in hypusination. *Structure* **2015,** *23* (5), 882-892.
19. Jasniewski, A. J.; Komor, A. J.; Lipscomb, J. D.; Que Jr, L., Unprecedented (μ-1,1-Peroxo)diferric Structure for the Ambiphilic Orange Peroxo Intermediate of the Nonheme *N*-Oxygenase CmlI. *Journal of the American Chemical Society* **2017,** *139* (30), 10472-10485.
20. Zhang, B.; Rajakovich, L. J.; Van Cura, D.; Blaesi, E. J.; Mitchell, A. J.; Tysoe, C. R.; Zhu, X.; Streit, B. R.; Rui, Z.; Zhang, W.; Boal, A. K.; Krebs, C.; Bollinger, J. M., Substrate-triggered Formation of a Peroxo-Fe_2(III/III) Intermediate during Fatty Acid Decarboxylation by UndA. *Journal of the American Chemical Society* **2019,** *141* (37), 14510-14514.
21. McBride, M.; Sil, D.; Ng, T. L.; Crooke, A. M.; Kenney, G. E.; Tysoe, C. R.; Zhang, B.; Balskus, E. P.; Boal, A. K.; Krebs, C., A peroxodiiron (III) intermediate mediating both N-hydroxylation steps in biosynthesis of the N-nitrosourea pharmacophore of streptozotocin by SznF. *Journal of the American Chemical Society* **2020**.
22. McBride, M.; Sil, D.; Ng, T. L.; Crooke, A. M.; Kenney, G. E.; Tysoe, C. R.; Zhang, B.; Balskus, E. P.; Boal, A. K.; Krebs, C., A peroxodiiron(III) intermediate mediating both *N*-hydroxylation steps in biosynthesis of the *N*-nitrosourea pharmacophore of streptozotocin by SznF. *Journal of the American Chemical Society* **2020,** *142* (27), 11818-11828.
23. Korboukh, V. K.; Li, N.; Barr, E. W.; Bollinger Jr, J. M.; Krebs, C., A long-lived, substrate-hydroxylating peroxodiiron (III/III) intermediate in the amine oxygenase, AurF, from Streptomyces thioluteus. *Journal of the American Chemical Society* **2009,** *131* (38), 13608-13609.
24. Korboukh, V. K.; Li, N.; Krebs, C.; Bollinger, J. M., Four-electron oxidation of p-hydroxylaminobenzoate to p-nitrobenzoate by a peroxodiferric complex in AurF from Streptomyces thioluteus. *Proceedings of the National Academy of Sciences* **2010,** *107* (36), 15722-15727.
25. Manley, O. M.; Fan, R.; Guo, Y.; Makris, T. M., Oxidative Decarboxylase UndA Utilizes a Dinuclear Iron Cofactor. *Journal of the American Chemical Society* **2019,** *141* (22), 8684-8688.